SIAM J. IMAGING SCIENCES
Vol. 12, No. 1, pp. 119–152

Uniqueness and Direct Imaging Method for Inverse Scattering by Locally Rough Surfaces with Phaseless Near-Field Data*

Xiaoxu Xu†, Bo Zhang‡, and Haiwen Zhang§

Abstract. This paper is concerned with inverse scattering of plane waves by a locally perturbed infinite plane (which is called a locally rough surface) with the modulus of the total-field data (also called the phaseless near-field data) at a fixed frequency in two dimensions. We consider the case where a Dirichlet boundary condition is imposed on the locally rough surface. This problem models inverse scattering of plane acoustic waves by a one-dimensional sound-soft, locally rough surface; it also models inverse scattering of plane electromagnetic waves by a locally perturbed, perfectly reflecting, infinite plane in the transverse electric polarization case. We prove that the locally rough surface is uniquely determined by the phaseless near-field data generated by a countably infinite number of plane waves and measured on an open domain above the locally rough surface. Further, a direct imaging method is proposed to reconstruct the locally rough surface from the phaseless near-field data generated by plane waves and measured on the upper part of the circle with a sufficiently large radius. Theoretical analysis of the imaging algorithm is derived by making use of properties of the scattering solution and results from the theory of oscillatory integrals (especially the method of stationary phase). Moreover, as a by-product of the theoretical analysis, a similar direct imaging method with full far-field data is also proposed to reconstruct the locally rough surface. Finally, numerical experiments are carried out to demonstrate that the imaging algorithms with phaseless near-field data and full far-field data are fast, accurate, and very robust with respect to noise in the data.

Key words. inverse scattering, locally rough surface, Dirichlet boundary condition, phaseless near-field data, full far-field data

AMS subject classifications. 35R30, 35Q60, 65R20, 65N21, 78A46

DOI. 10.1137/18M1210204

1. Introduction.

Acoustic and electromagnetic scattering by a locally perturbed infinite plane (called a locally rough surface in this paper) occurs in many applications such as radar, remote sensing, geophysics, medical imaging, and nondestructive testing (see, e.g., [3, 5, 8, 10, 13, 19]).

*Received by the editors August 28, 2018; accepted for publication (in revised form) November 29, 2018; published electronically January 22, 2019.

http://www.siam.org/journals/siims/12-1/M121020.html

Funding: The work of the authors was partially supported by National Natural Science Foundation of China grants 91630309, 11501558, 11571355, and 11871466.

†Academy of Mathematics and Systems Science, Chinese Academy of Sciences, Beijing 100190, China, and School of Mathematical Sciences, University of Chinese Academy of Sciences, Beijing 100049, China (xuxiaoxu14@mails.ucas.ac.cn).

‡NCMIS, LSEC, and Academy of Mathematics and Systems Science, Chinese Academy of Sciences, Beijing 100190, China, and School of Mathematical Sciences, University of Chinese Academy of Sciences, Beijing 100049, China (b.zhang@amt.ac.cn).

§NCMIS and Academy of Mathematics and Systems Science, Chinese Academy of Sciences, Beijing 100190, China (zhanghaiwen@amss.ac.cn).

In this paper, we are restricted to the two-dimensional case by assuming that the local perturbation is invariant in the x_3 direction. Assume further that the incident wave is time-harmonic ($e^{-i\omega t}$ time dependence), so that the total wave field u satisfies the Helmholtz equation

$$\Delta u + k^2 u = 0 \quad \text{in } D_+. \tag{1.1}$$

Here, $k = \omega/c > 0$ is the wave number, ω and c are the frequency and speed of the wave in D_+, respectively, and $D_+ := \{(x_1, x_2) \mid x_2 > h(x_1), x_1 \in \mathbb{R}\}$ represents a homogeneous medium above the locally rough surface denoted by $\Gamma := \partial D_+ = \{(x_1, x_2) \mid x_2 = h(x_1), x_1 \in \mathbb{R}\}$ with $h \in C^2(\mathbb{R})$ having a compact support in $\mathbb{R}$. In this paper, the incident field u^i is assumed to be the plane wave

$$u^i(x, d) := e^{ikx\cdot d}, \tag{1.2}$$

where $d = (\cos\theta_d, \sin\theta_d) \in \mathbb{S}^1_-$ is the incident direction with $\pi < \theta_d < 2\pi$ and $\mathbb{S}^1_- := \{x = (x_1, x_2) \mid |x| = 1, x_2 < 0\}$ is the lower part of the unit circle $\mathbb{S}^1 = \{x \in \mathbb{R}^2 \mid |x| = 1\}$. This paper considers the case where a Dirichlet boundary condition is imposed on the locally rough surface. Thus, the total field $u(x, d) = u^i(x, d) + u^r(x, d) + u^s(x, d)$ vanishes on the surface Γ,

$$u(x, d) = u^i(x, d) + u^r(x, d) + u^s(x, d) = 0 \qquad \text{on } \Gamma, \tag{1.3}$$

where u^r is the reflected wave by the infinite plane $x_2 = 0$,

$$u^r(x, d) := -e^{ikx\cdot d'} \tag{1.4}$$

with $d' = (\cos\theta_d, -\sin\theta_d)$ and u^s is the unknown scattered wave to be determined which is required to satisfy the Sommerfeld radiation condition

$$\lim_{r\to\infty} r^{\frac{1}{2}} \left(\frac{\partial u^s}{\partial r} - iku^s \right) = 0, \quad r = |x|, \quad x \in D_+. \tag{1.5}$$

This problem models electromagnetic scattering by a locally perturbed, perfectly conducting, infinite plane in the transverse electric polarization case; it also models acoustic scattering by a one-dimensional sound-soft, locally rough surface. See Figure 1.1 for the geometry of the scattering problem.

The well-posedness of the scattering problem (1.1)–(1.5) has been studied by using the variational method with a Dirichlet-to-Neumann map in [5] or the integral equation method

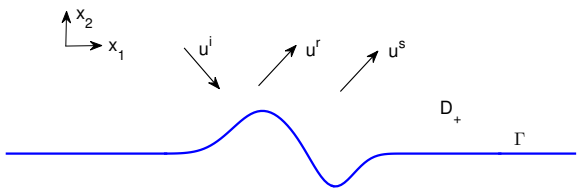

Figure 1.1. *The scattering problem from a locally rough surface.*

in [50, 54]. In particular, it was proved in [50, 54] that u^s has the asymptotic behavior at infinity

$$u^s(x,d) = \frac{e^{ik|x|}}{\sqrt{|x|}}\left(u^\infty(\hat{x},d) + O\Big(\frac{1}{|x|}\Big)\right), \qquad |x| \to \infty, \tag{1.6}$$

uniformly for all observation directions $\hat{x} := x/|x| \in \mathbb{S}^1_+$ with $\mathbb{S}^1_+ := \{x = (x_1, x_2) \mid |x| = 1, x_2 > 0\}$ the upper part of the unit circle $\mathbb{S}^1$, where $u^\infty(\hat{x}, d)$ is called the far-field pattern of the scattered field u^s, depending on the observation direction $\hat{x} \in \mathbb{S}^1_+$ and the incident direction $d \in \mathbb{S}^1_-$.

Many numerical algorithms have been proposed for the inverse problem of reconstructing the rough surfaces from the phased near-field or far-field data (see, e.g., [5, 8, 12, 17, 19, 20, 21, 31, 36, 37, 48, 54] and the references quoted there). For the case when the local perturbation is below the infinite plane which is called the inverse cavity problem, see [3, 35] and the references quoted there.

In diffractive optics and radar imaging, it is much harder to obtain data with accurate phase information compared with only measuring the intensity (or the modulus) of the data [4, 6, 13, 15, 30, 41, 46]. Thus it is often desirable to study inverse scattering problems with phaseless data. Inverse scattering with phaseless near-field data has been extensively studied numerically over the past decades (see, e.g., [4, 7, 14, 15, 16, 42, 46, 49] and the references quoted there). Recently, mathematical issues including uniqueness and stability have also been studied for inverse scattering with phaseless near-field data (see, e.g., [26, 27, 28, 29, 41, 43, 44] and the references quoted there).

In contrast to the case with phaseless near-field data, inverse scattering with phaseless far-field data is much less studied both mathematically and numerically due to the *translation invariance property* of the phaseless far-field data, that is, the modulus of the far-field pattern is invariant under translations of the obstacle for plane wave incidence [30, 38, 55]. The translation invariance property makes it impossible to reconstruct the location of the obstacle or the inhomogeneous medium from the phaseless far-field pattern with one plane wave as the incident field. Nevertheless, several reconstruction algorithms have been developed to reconstruct the shape of the obstacle from the phaseless far-field data with one plane wave as the incident field (see [1, 22, 23, 24, 30, 32, 33, 47]). Uniqueness has also been established in recovering the shape of the obstacle from the phaseless far-field data with one plane wave as the incident field [39, 40]. Recently, progress has been made on the mathematical and numerical study of inverse scattering with phaseless far-field data. For example, it was first proved in [55] that the translation invariance property of the phaseless far-field pattern can be broken by using superpositions of two plane waves as the incident fields for all wave numbers in a finite interval. And a recursive Newton-type iteration algorithm in frequencies was further developed in [55] to numerically reconstruct both the location and the shape of the obstacle simultaneously from multifrequency phaseless far-field data. This method was further extended in [56] to reconstruct the locally rough surface from multifrequency phaseless far-field or near-field data. Furthermore, a direct imaging algorithm was recently developed in [57] to reconstruct the obstacle from the phaseless far-field data generated by infinitely many sets of superpositions of two plane waves as the incident fields at a fixed frequency.

And uniqueness results have also been established rigorously in [51] for inverse obstacle and medium scattering from the phaseless far-field patterns generated by infinitely many sets of superpositions of two plane waves with different directions at a fixed frequency under certain a priori conditions on the obstacle and the inhomogeneous medium. The a priori assumption on the obstacle and the inhomogeneous medium in [51] was removed in [52] by adding a known reference ball into the scattering model. It should be noted that the reference-ball technique was first introduced to inverse scattering problems in a different but related context in [34] and then used in [58] to prove uniqueness results for inverse scattering with phaseless far-field data generated by superpositions of a plane wave and a point source as the incident fields at a fixed frequency; moreover, it was recently applied to inverse source scattering problems with phaseless data in [59]. Note further that by adding one point scatterer into the scattering model stability estimates have been obtained in [25] for inverse obstacle and medium scattering with phaseless far-field data associated with one plane wave as the incident field under certain conditions on the obstacle and inhomogeneous medium if the point scatterer is placed far away from the scatterer. In addition, direct imaging algorithms are proposed in [25] to reconstruct the scattering obstacle from the phaseless far-field data associated with one plane wave as the incident field.

In this paper, we consider uniqueness and the fast imaging algorithm for inverse scattering by locally rough surfaces from phaseless near-field data corresponding to incident plane waves at a fixed frequency. First, we prove that the locally rough surface is uniquely determined by the phaseless near-field data generated by a countably infinite number of incident plane waves and measured on an open domain above the locally rough surface, following the ideas in [43, 54]. Then we develop a direct imaging algorithm for the inverse scattering problem with phaseless near-field data generated by incident plane waves and measured on the upper part of the circle containing the local perturbation part of the infinite plane, based on the imaging function $I^{Phaseless}(z)$ with $z \in \mathbb{R}^2$ (see the formula (3.1) below). The theoretical analysis of the imaging function $I^{Phaseless}(z)$ is given by making use of properties of the scattering solution and results from the theory of oscillatory integrals (especially the method of stationary phase). From the theoretical analysis result, it is expected that if the radius of the measurement circle is sufficiently large, $I^{Phaseless}(z)$ will take a large value when z is on the boundary Γ and decay as z moves away from Γ. Based on this, a direct imaging algorithm is proposed to recover the locally rough surface from the phaseless near-field data. Further, numerical experiments are also carried out to demonstrate that our imaging algorithm provides an accurate, fast, and stable reconstruction of the locally rough surface. Moreover, as a by-product of the theoretical analysis, a similar direct imaging algorithm with full far-field data is also proposed to reconstruct the locally rough surfaces with convincing numerical experiments illustrating the effectiveness of the imaging algorithm. It should be pointed out that a direct imaging method was recently proposed in [14, 15] for reconstructing extended obstacles with acoustic and electromagnetic phaseless near-field data, based on the reverse time migration technique

The rest of the paper is organized as follows. The uniqueness result is proved in section 2 for an inverse scattering problem with phaseless near-field data. In section 3, the direct imaging method with phaseless near-field data is proposed, and its theoretical analysis is given. As a by-product, the direct imaging method with full far-field data is also presented in section 3. Numerical experiments are carried out in section 4 to illustrate the effectiveness of

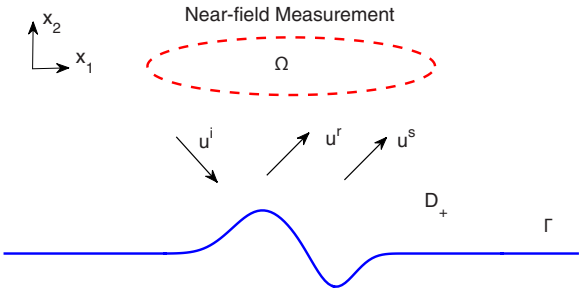

Figure 2.1. *Inverse scattering with phaseless near-field data measured on the domain* Ω.

the imaging method. Conclusions are given in section 5. In Appendix A, we use the method of stationary phase to prove Lemma 3.8 in section 3, which plays an important role in the theoretical analysis of the direct imaging method.

2. Uniqueness for an inverse problem. In this section, we establish a uniqueness result for an inverse scattering problem with phaseless near-field data, motivated by [43]. First, we introduce some notation which will be used throughout this paper. Define $B_R := \{x = (x_1, x_2) \mid |x| < R\}$ to be a disk centered at the origin and with radius $R > 0$ large enough so that the local perturbation $\Gamma_p := \{(x_1, h(x_1)) \mid x_1 \in \text{supp}(h)\} \subset B_R$. Define $\mathbb{R}^2_\pm := \{(x_1, x_2) \in \mathbb{R}^2 \mid x_2 \gtrless 0\}$, $\partial B_R^+ := \partial B_R \cap D_+$. For any $x, z \in \mathbb{R}^2$ and $d \in \mathbb{S}^1$, set $x := (x_1, x_2), z := (z_1, z_2), d := (d_1, d_2)$ and let $x' := (x_1, -x_2)$ be the reflection of x with respect to the x_1-axis. Further, let $\hat{x} = x/|x| = (\hat{x}_1, \hat{x}_2) = (\cos\theta_{\hat{x}}, \sin\theta_{\hat{x}})$, $\hat{z} = z/|z| = (\hat{z}_1, \hat{z}_2) = (\cos\theta_{\hat{z}}, \sin\theta_{\hat{z}})$ and $d = (\cos\theta_d, \sin\theta_d)$ with $\theta_{\hat{x}}, \theta_{\hat{z}}, \theta_d \in [0, 2\pi]$. Note also that if $x \neq 0$, then $\hat{x}_1 = x_1/|x|$ and $\hat{x}_2 = x_2/|x|$. Throughout this paper, the positive constants C, C_1, and C_2 may be different at different places.

Assume that Γ_1, Γ_2 are two locally rough surfaces, where $\Gamma_j := \{(x_1, x_2) \mid x_2 = h_j(x_1), x_1 \in \mathbb{R}\}$ with $h_j \in C^2(\mathbb{R})$ having a compact support in $\mathbb{R}$, $j = 1, 2$. Further, denote by $\Gamma_{p,j} := \{(x_1, h_j(x_1)) \mid x_1 \in \text{supp}(h_j)\}$ the local perturbation of Γ_j and by $D_{+,j}$ the domain above Γ_j, $j = 1, 2$. For $j = 1, 2$ suppose that the total field is given by $u_j = u^r + u^r + u_j^s$, where $u_j^s(\hat{x}, d)$ is the scattered field corresponding to the locally rough surface Γ_j with its far-field pattern $u_j^\infty(\hat{x}, d)$. Moreover, let $R > 0$ be large enough such that the local perturbation $\Gamma_{p,j} \subset B_R$ $(j = 1, 2)$ and let Ω be a bounded open domain above the locally rough surfaces Γ_1 and Γ_2. See Figure 2.1 for the geometry of the inverse scattering problem.

We need the following result on the property of the scattered field, which is also useful in the numerical algorithm in section 3.

Lemma 2.1. *Let* $x \in D_+$, $d \in \mathbb{S}^1_-$. *Then for any* $x \in D_+$ *with* $|x|$ *large enough and* $d \in \mathbb{S}^1_-$ *the scattering solution* $u^s(x, d)$ *of the scattering problem* (1.1)–(1.5) *has the asymptotic behavior*

$$u^s(x, d) = \frac{e^{ik|x|}}{|x|^{1/2}} u^\infty(\hat{x}, d) + u^s_{Res}(x, d) \tag{2.1}$$

with

$$\|u^\infty(\cdot,d)\|_{C^1(\mathbb{S}^1_+)} \le C, \tag{2.2}$$

$$|u^s_{Res}(x,d)| \le \frac{C}{|x|^{3/2}}, \tag{2.3}$$

where $C>0$ is a constant independent of x and d.

Proof. The statement of this lemma follows easily from the well-posedness of the scattering problem (1.1)–(1.5) and the asymptotic behavior (1.6) of the scattered field u^s (see, e.g., [54]). ∎

We also need the following uniqueness result for the inverse scattering problem with full far-field data which is given in [54].

Theorem 2.2 (Theorem 4.1 in [54]). *Assume that Γ_1 and Γ_2 are two locally rough surfaces and $u_1^\infty(\hat{x},d)$ and $u_2^\infty(\hat{x},d)$ are the far-field patterns corresponding to Γ_1 and Γ_2, respectively. If $u_1^\infty(\hat{x},d_n)=u_2^\infty(\hat{x},d_n)$ for all $\hat{x}\in\mathbb{S}^1_+$ and the distinct directions $d_n\in\mathbb{S}^1_-$ with $n\in\mathbb{N}$ and a fixed wave number k, then $\Gamma_1=\Gamma_2$.*

We are now ready to state and prove the main theorem of this section.

Theorem 2.3. *Assume that Γ_1 and Γ_2 are two locally rough surfaces and $u_1(\hat{x},d)$ and $u_2(\hat{x},d)$ are the total field corresponding to Γ_1 and Γ_2, respectively. Let Ω be a bounded open domain above Γ_1 and Γ_2. If $|u_1(x,d_n)|=|u_2(x,d_n)|$ for all $x\in\Omega$ and the distinct directions $d_n\in\mathbb{S}^1_-$ with $n\in\mathbb{N}$ and a fixed wave number k, then $\Gamma_1=\Gamma_2$.*

Proof. Fix $d=d_n$ for an arbitrary $n\in\mathbb{N}$ and set $d=(d_1,d_2)$. Since $|u_1(x,d)|=|u_2(x,d)|$ for all $x\in\Omega$, it follows from the analyticity of $|u_l(x,d)|^2$, $l=1,2$, with respect to $x\in\mathbb{R}^2_+\backslash\overline{B_R}$ that

$$|u_1(x,d)|=|u_2(x,d)| \quad \text{for } x\in\mathbb{R}^2_+\backslash\overline{B_R}. \tag{2.4}$$

Noting that $u_l=u^i+u^r+u^s_l$, $l=1,2$, we have

$$|u_l|^2=|u^i+u^r+u^s_l|^2=|u^i+u^r|^2+|u^s_l|^2+2\mathrm{Re}(u^i\overline{u^s_l})+2\mathrm{Re}(u^r\overline{u^s_l}). \tag{2.5}$$

Now, by Lemma 2.1 we know that for $x\in D_{+,l}$,

$$u^s_l(x,d)=\frac{e^{ik|x|}}{|x|^{1/2}}u^\infty_l(\hat{x},d)+u^s_{l,Res}(x,d), \quad l=1,2, \tag{2.6}$$

with

$$|u^s_{l,Res}(x,d)|\le C|x|^{-3/2}, \qquad |u^s_l(x,d)|\le C|x|^{-1/2} \tag{2.7}$$

for $|x|$ large enough.

Write

$$u^\infty_l(\hat{x},d)=r_l(\hat{x},d)e^{i\theta_l(\hat{x},d)}, \quad l=1,2, \tag{2.8}$$

where $r_l(\hat{x},d), \theta_l(\hat{x},d)$ are real-valued functions with $r_l \geq 0$ and $\theta_l \in [0,2\pi]$. Then, by inserting (2.6) and (2.8) into (2.5) we obtain that for $l=1,2$,

$$\begin{aligned}|u_l(x,d)|^2 &= |u^i(x,d)+u^r(x,d)|^2 + |u_l^s(x,d)|^2 + 2\mathrm{Re}\left(u^i(x,d)\overline{u^s_{l,Res}(x,d)}\right)\\ &\quad + 2\mathrm{Re}\left(u^i(x,d)\frac{e^{-ik|x|}}{|x|^{1/2}}r_l(\hat{x},d)e^{-i\theta_l(\hat{x},d)}\right) + 2\mathrm{Re}\left(u^r(x,d)\overline{u^s_{l,Res}(x,d)}\right)\\ &\quad + 2\mathrm{Re}\left(u^r(x,d)\frac{e^{-ik|x|}}{|x|^{1/2}}r_l(\hat{x},d)e^{-i\theta_l(\hat{x},d)}\right).\end{aligned}$$

This yields

$$\begin{aligned}&\frac{|x|^{1/2}}{2}\left(|u_l(x,d)|^2 - |u^i(x,d)+u^r(x,d)|^2\right)\\ &\quad = \mathrm{Re}\left(u^i(x,d)r_l(\hat{x},d)e^{-i(k|x|+\theta_l(\hat{x},d))}\right)\\ &\quad\quad + \mathrm{Re}\left(u^r(x,d)r_l(\hat{x},d)e^{-i(k|x|+\theta_l(\hat{x},d))}\right) + v_l(x,d),\end{aligned} \tag{2.9}$$

where v_l is given by

$$v_l(x,d) = |x|^{1/2}\left[\frac{1}{2}|u_l^s(x,d)|^2 + \mathrm{Re}\left(u^i(x,d)\overline{u^s_{l,Res}(x,d)}\right) + \mathrm{Re}\left(u^r(x,d)\overline{u^s_{l,Res}(x,d)}\right)\right].$$

Further, by (2.7) we see that for $l=1,2$,

$$|v_l(x,d)| \leq \frac{C}{|x|^{1/2}} \quad \text{as} \quad |x| \to +\infty. \tag{2.10}$$

Substituting (1.2) and (1.4) into (2.9) gives that for $x \in \mathbb{R}^2_+ \backslash \overline{B_R}$,

$$\begin{aligned}&\frac{|x|^{1/2}}{4}(|u_l(x,d)|^2 - |u^i(x,d)+u^r(x,d)|^2)\\ &= \frac{1}{2}r_l(\hat{x},d)\left[\cos(kx\cdot d - k|x| - \theta_l(\hat{x},d)) - \cos(kx\cdot d' - k|x| - \theta_l(\hat{x},d))\right] + \frac{1}{2}v_l(x,d)\\ &= r_l(\hat{x},d)\sin(k\hat{x}_2d_2|x|)\sin(\theta_l(\hat{x},d)+|x|(k-k\hat{x}_1d_1)) + \frac{1}{2}v_l(x,d), \quad l=1,2.\end{aligned} \tag{2.11}$$

Thus, and by (2.4) we have that for $x \in \mathbb{R}^2_+ \backslash \overline{B_R}$,

$$\begin{aligned}&r_1(\hat{x},d)\sin(k\hat{x}_2d_2|x|)\sin[\theta_1(\hat{x},d)+|x|(k-k\hat{x}_1d_1)] + \frac{1}{2}v_1(x,d)\\ &\quad = r_2(\hat{x},d)\sin(k\hat{x}_2d_2|x|)\sin[\theta_2(\hat{x},d)+|x|(k-k\hat{x}_1d_1)] + \frac{1}{2}v_2(x,d).\end{aligned} \tag{2.12}$$

Arbitrarily fix $\hat{x}=(\hat{x}_1,\hat{x}_2) \in \mathbb{S}^1_+$ and set $\alpha = k\hat{x}_2d_2$ and $\beta = k(1-\hat{x}_1d_1)$. Equation (2.12) then becomes

$$\begin{aligned}&r_1(\hat{x},d)\sin(\alpha|x|)\sin[\theta_1(\hat{x},d)+\beta|x|] + \frac{1}{2}v_1(x,d)\\ &\quad = r_2(\hat{x},d)\sin(\alpha|x|)\sin[\theta_2(\hat{x},d)+\beta|x|] + \frac{1}{2}v_2(x,d).\end{aligned} \tag{2.13}$$

Note that $\alpha < 0, \beta > 0$ since $\hat{x} = (\hat{x}_1, \hat{x}_2) \in \mathbb{S}^1_+$ and $d = (d_1, d_2) \in \mathbb{S}^1_-$. Then we can choose $\gamma_0^{(1)}, \gamma_0^{(2)} \in \mathbb{R}$ such that

$$\sin\left(\frac{\alpha}{\beta}\gamma_0^{(k)}\right) \neq 0, \quad k = 1, 2, \tag{2.14}$$

$$\sin(\gamma_0^{(1)} - \gamma_0^{(2)}) \neq 0. \tag{2.15}$$

We now prove that

$$r_1 \sin(\theta_1 + \gamma_0^{(k)}) = r_2 \sin(\theta_2 + \gamma_0^{(k)}), \quad k = 1, 2, \tag{2.16}$$

where we write $r_l = r_l(\hat{x}, d)$, $\theta_l = \theta_l(\hat{x}, d)$, $l = 1, 2$, for simplicity. We distinguish between the following two cases.

Case 1. α/β is a rational number. In this case, it is easily seen that there exist $p_j \in \mathbb{N}$ with $j = 1, 2, \ldots$ such that $(\alpha/\beta)p_j \in \mathbb{N}$ and $\lim_{j\to+\infty} p_j = +\infty$. For $k = 1, 2$ let $x_j^{(k)} := (\gamma_0^{(k)} + 2\pi p_j)\hat{x}/\beta$. Then it is easy to see that $x_j^{(k)} \in \mathbb{R}^2_+ \backslash \overline{B}_R$ for large j and $\lim_{j\to+\infty} |x_j^{(k)}| = +\infty$. Thus, take $x = x_j^{(k)}$ with large j in (2.13) to obtain that

$$r_1 \sin\left(\frac{\alpha}{\beta}\gamma_0^{(k)}\right) \sin(\theta_1 + \gamma_0^{(k)}) + \frac{1}{2} v_1(x_j^{(k)}, d) = r_2 \sin\left(\frac{\alpha}{\beta}\gamma_0^{(k)}\right) \sin(\theta_2 + \gamma_0^{(k)}) + \frac{1}{2} v_2(x_j^{(k)}, d).$$

The required equality (2.16) then follows by taking $j \to +\infty$ in the above equation and using (2.10) and (2.14).

Case 2. α/β is an irrational number. In this case, by Kronecker's approximation theorem (see, e.g., [2, Theorem 7.7]), we know that there exist $p_j \in \mathbb{N}$ with $j = 1, 2, \ldots$ such that $(\alpha/\beta)p_j = m_j + a_j$ with $m_j \in \mathbb{N}$, $\lim_{j\to+\infty} a_j = 0$, and $\lim_{j\to+\infty} p_j = +\infty$. For $k = 1, 2$ let $x_j^{(k)}$ be defined as in Case 1. Then, similarly as in Case 1, take $x = x_j^{(k)}$ with large j in (2.13) to deduce that

$$\begin{aligned} &r_1 \sin\left(\frac{\alpha}{\beta}\gamma_0^{(k)} + 2\pi a_j\right) \sin(\theta_1 + \gamma_0^{(k)}) + \frac{1}{2} v_1(x_j^{(k)}, d) \\ &\quad = r_2 \sin\left(\frac{\alpha}{\beta}\gamma_0^{(k)} + 2\pi a_j\right) \sin(\theta_2 + \gamma_0^{(k)}) + \frac{1}{2} v_2(x_j^{(k)}, d). \end{aligned}$$

Thus, (2.16) also follows by letting $j \to +\infty$ in the above equation and using (2.10) and (2.14).

Finally, it follows from (2.16) and the arbitrariness of $\hat{x}, d$ that

$$\begin{pmatrix} \cos\gamma_0^{(1)}(\hat{x}, d_n) & \sin\gamma_0^{(1)}(\hat{x}, d_n) \\ \cos\gamma_0^{(2)}(\hat{x}, d_n) & \sin\gamma_0^{(2)}(\hat{x}, d_n) \end{pmatrix} \begin{pmatrix} r_1(\hat{x}, d_n)\sin\theta_1(\hat{x}, d_n) - r_2(\hat{x}, d_n)\sin\theta_2(\hat{x}, d_n) \\ r_1(\hat{x}, d_n)\cos\theta_1(\hat{x}, d_n) - r_2(\hat{x}, d_n)\cos\theta_2(\hat{x}, d_n) \end{pmatrix} = 0$$

for all $\hat{x} \in \mathbb{S}^1_+$ and $d_n \in \mathbb{S}^1_-$ with $n \in \mathbb{N}$. Condition (2.15) means that the determinant of the square matrix on the left of the above matrix equation does not vanish, and so the above matrix equation only has a trivial solution, that is,

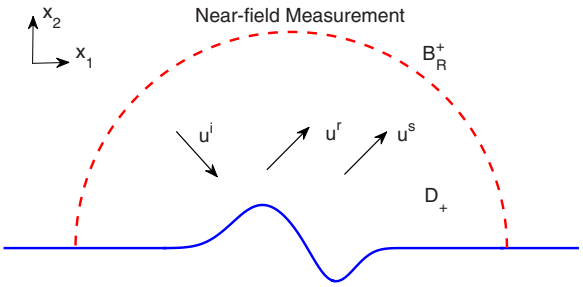

Figure 3.1. *Inverse scattering with phaseless near-field data measured on the curve* ∂B_R^+.

$$r_1(\hat{x}, d_n)\sin\theta_1(\hat{x}, d_n) = r_2(\hat{x}, d_n)\sin\theta_2(\hat{x}, d_n),$$
$$r_1(\hat{x}, d_n)\cos\theta_1(\hat{x}, d_n) = r_2(\hat{x}, d_n)\cos\theta_2(\hat{x}, d_n)$$

for all $\hat{x} \in \mathbb{S}_+^1$ and $d_n \in \mathbb{S}_-^1$ with $n \in \mathbb{N}$. This implies that $u_1^\infty(\hat{x}, d_n) = u_2^\infty(\hat{x}, d_n)$ for all $\hat{x} \in \mathbb{S}_+^1$ and $d_n \in \mathbb{S}_-^1$ with $n \in \mathbb{N}$. The required result then follows from Theorem 2.2. The proof is thus completed. ∎

3. Direct imaging method for inverse problems. In this section, we consider the inverse problem: Given the incident field $u^i = u^i(x, d)$, reconstruct the locally rough surface Γ from the phaseless near-field data $|u(x, d)|$ for all $x \in \partial B_R^+, d \in \mathbb{S}_-^1$ and with a fixed wave number k. See Figure 3.1 for the geometry of the inverse scattering problem. Our purpose is to develop a direct imaging method to solve this inverse problem numerically though no rigorous uniqueness result is available yet for the inverse problem.

We consider the imaging function

$$I^{Phaseless}(z) := \int_{\partial B_R^+} \left| \int_{\mathbb{S}_-^1} \left[\left(|u(x,d)|^2 - 2 + e^{2ikx_2d_2} \right) e^{ik(x-z)\cdot d} - e^{ik(x'-z')\cdot d} \right] ds(d) \right|^2 dx \tag{3.1}$$

for $z \in \mathbb{R}^2$. In what follows, we will study the behavior of the imaging function $I^{Phaseless}(z)$ for z near and away from the rough surface Γ. To this end, we will prove that if the radius R is sufficiently large, then $I^{Phaseless}(z) \approx F(R, z)$ for z in a bounded domain containing the local perturbation of the locally rough surface, where $F(R, z)$ is defined by (3.35) (see Theorem 3.9). From this, Theorem 3.10, and the discussions in [37, section 3], it is expected that if R is large enough, then the imaging function $I^{Phaseless}(z)$ will take a large value when $z \in \Gamma$ and decay as z moves away from Γ (more detailed discussions can be found following the proof of Theorem 3.10).

Define

$$U(x, z) := U_1(x, z) + U_2(x, z) + U_3(x, z), \tag{3.2}$$

$$W(x, z) := W_1(x, z) + W_2(x, z) + W_3(x, z) + W_4(x, z), \tag{3.3}$$

where

$$U_1(x,z) = \int_{\mathbb{S}^1_-} u^s(x,d)e^{-ikz\cdot d}ds(d), \tag{3.4}$$

$$U_2(x,z) = -\int_{\mathbb{S}^1_-} e^{ik(x\cdot d'-z\cdot d)}ds(d), \tag{3.5}$$

$$U_3(x,z) = -\int_{\mathbb{S}^1_-} e^{ik(x\cdot d'-z'\cdot d)}ds(d), \tag{3.6}$$

and

$$W_1(x,z) = \int_{\mathbb{S}^1_-} \left[u^i(x,d)\right]^2 \overline{u^s(x,d)}e^{-ikz\cdot d}ds(d),$$

$$W_2(x,z) = \int_{\mathbb{S}^1_-} u^i(x,d)u^r(x,d)\overline{u^s(x,d)}e^{-ikz\cdot d}ds(d),$$

$$W_3(x,z) = \int_{\mathbb{S}^1_-} u^i(x,d)\overline{u^r(x,d)}u^s(x,d)e^{-ikz\cdot d}ds(d),$$

$$W_4(x,z) = \int_{\mathbb{S}^1_-} u^i(x,d)|u^s(x,d)|^2e^{-ikz\cdot d}ds(d).$$

Since $u = u^i + u^r + u^s$ and $|u^i| = |u^r| = 1$, by a direct calculation (3.1) becomes

$$I^{Phaseless}(z) = \int_{\partial B_R^+} |U(x,z) + W(x,z)|^2 dx. \tag{3.7}$$

We need the following result for oscillatory integrals proved in [14].

Lemma 3.1 (Lemma 3.9 in [14]). *For any $-\infty < a < b < \infty$ let $u \in C^2[a,b]$ be real-valued and satisfy that $|u'(t)| \geq 1$ for all $t \in (a,b)$. Assume that $a = x_0 < x_1 < \cdots < x_N = b$ is a division of (a,b) such that u' is monotone in each interval (x_{i-1}, x_i), $i = 1, \ldots, N$. Then for any function ϕ defined on (a,b) with integrable derivative and for any $\lambda > 0$,*

$$\left|\int_a^b e^{i\lambda u(t)}\phi(t)dt\right| \leq (2N+2)\lambda^{-1}\left[|\phi(b)| + \int_a^b |\phi'(t)|dt\right].$$

With the aid of Lemma 3.1, we can obtain the following lemma.

Lemma 3.2. *Let $x \in \mathbb{R}^2_+$, $d \in \mathbb{S}^1_-$. For $\hat{x} = x/|x| \in \mathbb{S}^1_+$ assume that $f(\hat{x},\cdot)$, $g(\hat{x},\cdot) \in C^1(\overline{\mathbb{S}^1_-})$ and define*

$$F(x) := \int_{\mathbb{S}^1_-} e^{ikx\cdot d}f(\hat{x},d)ds(d), \qquad G(x) := \int_{\mathbb{S}^1_-} e^{ikx\cdot d'}g(\hat{x},d)ds(d).$$

Then for all $x \in \mathbb{R}^2_+$ with $|x|$ large enough we have

$$|F(x)| \leq C\|f(\hat{x},\cdot)\|_{C^1(\overline{\mathbb{S}^1_-})}|x|^{-1/2}, \tag{3.8}$$

$$|G(x)| \leq C\|g(\hat{x},\cdot)\|_{C^1(\overline{\mathbb{S}^1_-})}|x|^{-1/2}, \tag{3.9}$$

where $C > 0$ is a constant independent of x.

Proof. We prove only (3.8). The proof of (3.9) is similar.

Let $\delta > 0$ be small enough such that $\sin\delta \geq \delta/2$ and let $|x|$ be large enough. Let $x = |x|\hat{x} = |x|(\cos\theta_{\hat{x}}, \sin\theta_{\hat{x}})$, $d = (\cos\theta_d, \sin\theta_d)$ with $\theta_{\hat{x}} \in [0,\pi]$, $\theta_d \in [\pi, 2\pi]$, and define $\widetilde{f}(\theta_{\hat{x}}, \theta_d) := f(\hat{x}, d)$ for $\theta_{\hat{x}} \in [0,\pi]$ and $\theta_d \in [\pi, 2\pi]$. Then it follows that

$$C_1\|f(\hat{x},\cdot)\|_{C^1(\overline{\mathbb{S}^1_-})} \leq \|\widetilde{f}(\theta_{\hat{x}},\cdot)\|_{C^1[\pi,2\pi]} \leq C_2\|f(\hat{x},\cdot)\|_{C^1(\overline{\mathbb{S}^1_-})} \tag{3.10}$$

and

$$F(x) = \int_\pi^{2\pi} e^{ik|x|\cos(\theta_d-\theta_{\hat{x}})}\widetilde{f}(\theta_{\hat{x}},\theta_d)d\theta_d. \tag{3.11}$$

We distinguish between the following two cases.

Case 1. $\theta_{\hat{x}} \in [0,\delta] \cup [\pi-\delta,\pi]$. In this case, we rewrite (3.11) as

$$\begin{aligned} F(x) \;=\; & \int_{\pi+2\delta}^{2\pi-2\delta} e^{ik|x|\cos(\theta_d-\theta_{\hat{x}})}\widetilde{f}(\theta_{\hat{x}},\theta_d)d\theta_d + \int_\pi^{\pi+2\delta} e^{ik|x|\cos(\theta_d-\theta_{\hat{x}})}\widetilde{f}(\theta_{\hat{x}},\theta_d)d\theta_d \\ & + \int_{2\pi-\delta}^{2\pi} e^{ik|x|\cos(\theta_d-\theta_{\hat{x}})}\widetilde{f}(\theta_{\hat{x}},\theta_d)d\theta_d \\ :=\; & I_1 + II_1 + III_1. \end{aligned} \tag{3.12}$$

Set $u(\theta_d) = 2\cos(\theta_d-\theta_{\hat{x}})/\delta$. Then $u'(\theta_d) = -2\sin(\theta_d-\theta_{\hat{x}})/\delta$, and so, for $\theta_{\hat{x}} \in [0,\delta]\cup[\pi-\delta,\pi]$ and $\theta_d \in [\pi+2\delta, 2\pi-2\delta]$, we have

$$|u'(\theta_d)| = 2|\sin(\theta_d-\theta_{\hat{x}})|/\delta \geq 2|\sin\delta|/\delta \geq \frac{2}{\delta}\frac{\delta}{2} = 1$$

and $u'(\theta_d)$ is monotone in $[\pi+2\delta, 2\pi-2\delta]$. Thus, by Lemma 3.1 it follows that

$$|I_1| = \left|\int_{\pi+2\delta}^{2\pi-2\delta} e^{i\frac{\delta k|x|}{2}u(\theta_d)}\widetilde{f}(\theta_{\hat{x}},\theta_d)d\theta_d\right| \leq C\frac{\|\widetilde{f}(\theta_{\hat{x}},\cdot)\|_{C^1[\pi,2\pi]}}{\delta|x|}. \tag{3.13}$$

It is easy to obtain that

$$|II_1| + |III_1| \leq C\delta\|\widetilde{f}(\theta_{\hat{x}},\cdot)\|_{C^1[\pi,2\pi]}. \tag{3.14}$$

Combining (3.10), (3.12), (3.13), and (3.14) gives

$$|F(x)| \leq C\left(\frac{1}{\delta|x|}+\delta\right)\|\widetilde{f}(\theta_{\hat{x}},\cdot)\|_{C^1[\pi,2\pi]} \leq C\left(\frac{1}{\delta|x|}+\delta\right)\|f(\hat{x},\cdot)\|_{C^1(\overline{\mathbb{S}^1_-})}.$$

From this (3.8) follows immediately on taking $\delta = |x|^{-1/2}$.

Case 2. $\theta_{\hat{x}} \in [\delta, \pi-\delta]$. In this case, we rewrite (3.11) as

$$\begin{aligned} F(x) \;=\; & \int_0^{\theta_{\hat{x}}-\delta} e^{ik|x|\cos(\theta_d-\theta_{\hat{x}})}\widetilde{f}(\theta_{\hat{x}},\theta_d)d\theta_d + \int_{\theta_{\hat{x}}+\delta}^{\pi} e^{ik|x|\cos(\theta_d-\theta_{\hat{x}})}\widetilde{f}(\theta_{\hat{x}},\theta_d)d\theta_d \\ & + \int_{\theta_{\hat{x}}-\delta}^{\theta_{\hat{x}}+\delta} e^{ik|x|\cos(\theta_d-\theta_{\hat{x}})}\widetilde{f}(\theta_{\hat{x}},\theta_d)d\theta_d \\ :=\; & I_2 + II_2 + III_2. \end{aligned}$$

Similarly as in the estimation of I_1, it is deduced that

$$|I_2| + |II_2| \leq \frac{C}{\delta|x|}\|\widetilde{f}(\theta_{\hat{x}}, \cdot)\|_{C^1[\pi,2\pi]}.$$

Now, it is straightforward to see that

$$|III_2| \leq C\delta\|\widetilde{f}(\theta_{\hat{x}}, \cdot)\|_{C^1[\pi,2\pi]}.$$

Then we arrive at

$$|F(x)| \leq C\left(\frac{1}{\delta|x|} + \delta\right)\|\widetilde{f}(\theta_{\hat{x}}, \cdot)\|_{C^1[\pi,2\pi]} \leq C\left(\frac{1}{\delta|x|} + \delta\right)\|f(\hat{x}, \cdot)\|_{C^1(\overline{\mathbb{S}^1_-})}.$$

Taking $\delta = |x|^{-1/2}$ in the above inequality gives (3.8). The proof is thus completed. ∎

We also need the following reciprocity relation of the far-field pattern.

Lemma 3.3. *For $\hat{x} \in \mathbb{S}^1_+$, $d \in \mathbb{S}^1_-$ let $u^\infty(\hat{x}, d)$ denote the far-field pattern of the scattering solution to the problem (1.1)–(1.5). Then $u^\infty(\hat{x}, d) = u^\infty(-d, -\hat{x})$ for all $\hat{x} \in \mathbb{S}^1_+$, $d \in \mathbb{S}^1_-$.*

Proof. The reciprocity relation of the far-field pattern has been proved in [18] for the case of bounded obstacles (see Theorem 3.15 in [18]). For the case of locally rough surfaces, the result can be proved similarly with minor modifications in conjunction with the integral equation method in [54]. ∎

We are now in a position to study the properties of U_i $(i = 1, 2, 3)$ and W_i $(i = 1, 2, 3, 4)$.

Lemma 3.4. *For arbitrarily fixed $z \in \mathbb{R}^2$ and for all $x \in \mathbb{R}^2_+$ with $|x|$ large enough, we have*

$$|U_1(x, z)| \leq C|x|^{-1/2}, \tag{3.15}$$

$$|U_i(x, z)| \leq C(1 + |z|)|x|^{-1/2}, \quad i = 2, 3, \tag{3.16}$$

$$|W_j(x, z)| \leq C|x|^{-1/2}, \quad j = 2, 3, \tag{3.17}$$

where $C > 0$ is a constant independent of x and z.

Proof. First, the estimates (3.15) and (3.17) follow easily from Lemma 2.1.

We now prove the estimate of $U_i(x, z)$, $i = 2, 3$, in (3.16). To this end, define $f_z(d) := -e^{-ikz\cdot d}$. Then

$$U_2(x, z) = \int_{\mathbb{S}^1_-} e^{ikx\cdot d'} f_z(d) ds(d).$$

Apply Lemma 3.2 to obtain that

$$|U_2(x, z)| \leq C\|f_z(\cdot)\|_{C^1(\overline{\mathbb{S}^1_-})}|x|^{-1/2} \leq C(1 + |z|)|x|^{-1/2}$$

for $x \in \mathbb{R}^2_+$ with $|x|$ large enough. The estimate for $U_3(x, z)$ can be obtained similarly. The proof is thus complete. ∎

Lemma 3.5. *For arbitrarily fixed $z \in \mathbb{R}^2$ and for all $x \in \mathbb{R}^2_+$ with $|x|$ large enough, we have*

$$|W_1(x,z)| \le C(1+|z|)|x|^{-1}, \tag{3.18}$$

$$|W_4(x,z)| \le C|x|^{-1}. \tag{3.19}$$

Here, $C > 0$ is a constant independent of x and z.

Proof. We first consider $W_1(x,z)$. From Lemma 2.1 it follows that for $x \in \mathbb{R}^2_+$ with $|x|$ large enough,

$$W_1(x,z) = \frac{e^{-ik|x|}}{|x|^{1/2}} \int_{\mathbb{S}^1_-} e^{2ikx\cdot d}\overline{u^\infty(\hat{x},d)}e^{-ikz\cdot d}ds(d) + W_{1,Res}(x,z), \tag{3.20}$$

where

$$W_{1,Res}(x,z) := \int_{\mathbb{S}^1_-} e^{2ikx\cdot d}\overline{u_{Res}(x,d)}e^{-ikz\cdot d}ds(d)$$

with

$$|W_{1,Res}(x,z)| \le C|x|^{-3/2}. \tag{3.21}$$

Now define

$$F(x) := \int_{\mathbb{S}^1_-} e^{2ikx\cdot d} f_z(\hat{x},d)ds(d)$$

with

$$f_z(\hat{x},d) := \overline{u^\infty(\hat{x},d)}e^{-ikz\cdot d}, \quad \hat{x} \in \mathbb{S}^1_+,\ d \in \mathbb{S}^1_-.$$

Then, by Lemmas 2.1, 3.2, and 3.3 we deduce that for $x \in \mathbb{R}^2_+$ with $|x|$ large enough,

$$\begin{aligned} |F(x)| &\le C\|f_z(\hat{x},\cdot)\|_{C^1(\overline{\mathbb{S}^1_-})}|x|^{-1/2} \\ &\le C(1+|z|)\|u^\infty(\hat{x},\cdot)\|_{C^1(\overline{\mathbb{S}^1_-})}|x|^{-1/2} \le C(1+|z|)|x|^{-\frac{1}{2}}. \end{aligned} \tag{3.22}$$

Thus, (3.18) follows immediately from (3.20), (3.21), and (3.22).

We now consider $W_4(x,z)$. By Lemma 2.1 we know that $|u^s(x,d)|^2 \le C/|x|$ for $x \in \mathbb{R}^2_+$ with $|x|$ large enough and $d \in \mathbb{S}^1_-$. Thus, (3.19) follows from the definition of $W_4(x,z)$. ∎

Lemma 3.6. *For arbitrarily fixed $z \in \mathbb{R}^2$ and for $R > 0$ large enough we have*

$$\left|\int_{\partial B_R^+} U(x,z)\overline{W_j(x,z)}dx\right| \le C\big(1+|z|\big)^2 R^{-1/2},$$

$$\int_{\partial B_R^+} |W_j(x,z)|^2 dx \le C(1+|z|)^2 R^{-1}$$

for $j = 1, 4$. Here, $C > 0$ is a constant independent of R and z.

Proof. From Lemmas 3.4 and 3.5 it follows that for $j = 1, 4$ and $R > 0$ large enough,

$$\left|\int_{\partial B_R^+} U(x,z)\overline{W_j(x,z)}dx\right| \le C\int_{\partial B_R^+} \frac{1+|z|}{R^{1/2}}\cdot\frac{1+|z|}{R}dx \le C\frac{(1+|z|)^2}{R^{1/2}},$$
$$\left|\int_{\partial B_R^+} |W_j(x,z)|^2 dx\right| \le C\int_{\partial B_R^+}\left(\frac{1+|z|}{R}\right)^2 dx \le C\frac{(1+|z|)^2}{R}.$$

The proof is thus complete. ∎

Lemma 3.7. *For arbitrarily fixed $z \in \mathbb{R}^2$ and for $R > 0$ large enough we have*

$$\sum_{i=1}^{3}\left|\int_{\partial B_R^+} U_i(x,z)\overline{W_j(x,z)}dx\right| + \sum_{i=1}^{4}\left|\int_{\partial B_R^+} W_i(x,z)\overline{W_j(x,z)}dx\right| \le C\frac{(1+|z|)^2}{R^{1/3}}$$

for $j = 2, 3$, where $C > 0$ is a constant independent of R and z.

Proof. From Lemma 2.1 it is easy to derive that for $x \in \mathbb{R}^2_+$ with $|x|$ large enough,

$$W_2(x,z) = -\frac{e^{-ik|x|}}{|x|^{1/2}}\int_{\mathbb{S}^1_-} e^{2ik|x|\hat{x}_1\cdot d_1}\overline{u^\infty(\hat{x},d)}e^{-ikz\cdot d}ds(d) + W_{2,Res}(x,z), \tag{3.23}$$

$$W_3(x,z) = -\frac{e^{ik|x|}}{|x|^{1/2}}\int_{\mathbb{S}^1_-} e^{2ik|x|\hat{x}_2\cdot d_2}u^\infty(\hat{x},d)e^{-ikz\cdot d}ds(d) + W_{3,Res}(x,z), \tag{3.24}$$

where

$$W_{2,Res}(x,z) := \int_{\mathbb{S}^1_-} e^{2ik|x|\hat{x}_1\cdot d_1}\overline{u^s_{Res}(x,d)}e^{-ikz\cdot d}ds(d),$$
$$W_{3,Res}(x,z) := \int_{\mathbb{S}^1_-} e^{2ik|x|\hat{x}_2\cdot d_2}u^s_{Res}(x,d)e^{-ikz\cdot d}ds(d)$$

with

$$|W_{j,Res}(x,z)| \le C|x|^{-3/2}, \quad j = 2, 3. \tag{3.25}$$

By Lemmas 3.4 and 3.5 we obtain that

$$\sum_{i=1}^{3}|U_i(x,z)| + \sum_{i=1}^{4}|W_i(x,z)| \le \frac{C(1+|z|)}{|x|^{1/2}}, \quad |x| \to +\infty. \tag{3.26}$$

Now, let $x = |x|\hat{x} = |x|(\cos\theta_{\hat{x}}, \sin\theta_{\hat{x}})$, $d = (\cos\theta_d, \sin\theta_d)$ with $\theta_{\hat{x}} \in [0,\pi]$, $\theta_d \in [\pi, 2\pi]$, and define $\widetilde{f}_z(\theta_{\hat{x}},\theta_d) := \overline{u^\infty(\hat{x},d)}e^{-ikz\cdot d}$, $\widetilde{g}_z(\theta_{\hat{x}},\theta_d) := u^\infty(\hat{x},d)e^{-ikz\cdot d}$ for $\theta_{\hat{x}} \in [0,\pi]$ and $\theta_d \in [\pi, 2\pi]$. Then it follows from (3.23), (3.24), (3.25), and (3.26) that

$$\sum_{i=1}^{3}\left|\int_{\partial B_R^+} U_i(x,z)\overline{W_2(x,z)}dx\right| + \sum_{i=1}^{4}\left|\int_{\partial B_R^+} W_i(x,z)\overline{W_2(x,z)}dx\right|$$

$$\le C(1+|z|)\left(\int_{\mathbb{S}_+^1}\left|\int_{\mathbb{S}_-^1} e^{2ikR\hat{x}_1\cdot d_1}\overline{u^\infty(\hat{x},d)}e^{-ikz\cdot d}ds(d)\right|ds(\hat{x}) + \frac{C}{R}\right)$$

$$= C(1+|z|)\left(\int_0^\pi\left|\int_\pi^{2\pi} e^{2ikR\cos\theta_{\hat{x}}\cos\theta_d}\widetilde{f}_z(\theta_{\hat{x}},\theta_d)d\theta_d\right|d\theta_{\hat{x}} + \frac{C}{R}\right), \tag{3.27}$$

$$\sum_{i=1}^{3}\left|\int_{\partial B_R^+} U_i(x,z)\overline{W_3(x,z)}dx\right| + \sum_{i=1}^{4}\left|\int_{\partial B_R^+} W_i(x,z)\overline{W_3(x,z)}dx\right|$$

$$\le C(1+|z|)\left(\int_{\mathbb{S}_+^1}\left|\int_{\mathbb{S}_-^1} e^{2ikR\hat{x}_2\cdot d_2}u^\infty(\hat{x},d)e^{-ikz\cdot d}ds(d)\right|ds(\hat{x}) + \frac{C}{R}\right)$$

$$= C(1+|z|)\left(\int_0^\pi\left|\int_\pi^{2\pi} e^{2ikR\sin\theta_{\hat{x}}\sin\theta_d}\widetilde{g}_z(\theta_{\hat{x}},\theta_d)d\theta_d\right|d\theta_{\hat{x}} + \frac{C}{R}\right). \tag{3.28}$$

Let $\varepsilon > 0$ be small enough such that $\sin\varepsilon \ge \varepsilon/2$ and let R be large enough. Define

$$\widetilde{w}_z(R,\theta_{\hat{x}}) := \int_\pi^{2\pi} e^{2ikR\cos\theta_{\hat{x}}\cos\theta_d}\widetilde{f}_z(\theta_{\hat{x}},\theta_d)d\theta_d$$

for $\theta_{\hat{x}} \in [0,\pi]$. Then, by Lemma 2.1 we have

$$\int_0^\pi |\widetilde{w}_z(R,\theta_{\hat{x}})|d\theta_{\hat{x}}$$

$$= \int_{[0,\frac{\pi}{2}-\varepsilon]\cup[\pi/2+\varepsilon,\pi]} |\widetilde{w}_z(R,\theta_{\hat{x}})|d\theta_{\hat{x}} + \int_{[\pi/2-\varepsilon,\pi/2+\varepsilon]} |\widetilde{w}_z(R,\theta_{\hat{x}})|d\theta_{\hat{x}}$$

$$\le C\varepsilon + \int_{[0,\pi/2-\varepsilon]\cup[\pi/2+\varepsilon,\pi]} |\widetilde{w}_z(R,\theta_{\hat{x}})|d\theta_{\hat{x}}$$

$$\le C\varepsilon + \int_{[0,\pi/2-\varepsilon]\cup[\pi/2+\varepsilon,\pi]}\left|\int_{[\pi+\varepsilon,2\pi-\varepsilon]} e^{2ikR\cos\theta_{\hat{x}}\cos\theta_d}\widetilde{f}_z(\theta_{\hat{x}},\theta_d)d\theta_d\right|d\theta_{\hat{x}}$$

$$+ \int_{[0,\pi/2-\varepsilon]\cup[\pi/2+\varepsilon,\pi]}\left|\int_{[\pi,\pi+\varepsilon]\cup[2\pi-\varepsilon,2\pi]} e^{2ikR\cos\theta_{\hat{x}}\cos\theta_d}\widetilde{f}_z(\theta_{\hat{x}},\theta_d)d\theta_d\right|d\theta_{\hat{x}}$$

$$\le C\varepsilon + \int_{[0,\pi/2-\varepsilon]\cup[\pi/2+\varepsilon,\pi]}\left|\int_{[\pi+\varepsilon,2\pi-\varepsilon]} e^{2ikR\cos\theta_{\hat{x}}\cos\theta_d}\widetilde{f}_z(\theta_{\hat{x}},\theta_d)d\theta_d\right|d\theta_{\hat{x}}. \tag{3.29}$$

Let $u_{\theta_{\hat{x}}}(\theta_d) = 4\varepsilon^{-2}\cos\theta_{\hat{x}}\cos\theta_d$. Then it is easy to see that $u'_{\theta_{\hat{x}}}(\theta_d) = -4\varepsilon^{-2}\cos\theta_{\hat{x}}\sin\theta_d$, and so we obtain that for $\theta_{\hat{x}} \in [0,\pi/2-\varepsilon]\cup[\pi/2+\varepsilon,\pi]$ and $\theta_d \in [\pi+\varepsilon,2\pi-\varepsilon]$,

$$|u'_{\theta_{\hat{x}}}(\theta_d)| = \frac{4}{\varepsilon^2}|\cos\theta_{\hat{x}}||\sin\theta_d| = \frac{4}{\varepsilon^2}|\sin(\theta_{\hat{x}}-\pi/2)||\sin\theta_d| \ge \frac{4}{\varepsilon^2}\sin^2\varepsilon \ge \frac{4}{\varepsilon^2}\left(\frac{\varepsilon}{2}\right)^2 = 1$$

and $u''_{\theta_{\hat{x}}}(\theta_d) = -4\varepsilon^{-2}\cos\theta_{\hat{x}}\cos\theta_d$ is monotone for $\theta_d \in [\pi+\varepsilon,2\pi-\varepsilon]$. Thus we can apply Lemmas 2.1, 3.1, and 3.3 to obtain that for $\theta_{\hat{x}} \in [0,\pi/2-\varepsilon]\cup[\pi/2+\varepsilon,\pi]$

$$
\begin{aligned}
&\left|\int_{[\pi+\varepsilon,2\pi-\varepsilon]} e^{2ikR\cos\theta_{\hat{x}}\cos\theta_d}\widetilde{f}_z(\theta_{\hat{x}},\theta_d)d\theta_d\right| \\
&\quad=\left|\int_{[\pi+\varepsilon,2\pi-\varepsilon]} e^{(ikR\varepsilon^2/2)u_{\theta_{\hat{x}}}(\theta_d)}\widetilde{f}_z(\theta_{\hat{x}},\theta_d)d\theta_d\right| \\
&\quad\le\frac{C}{R\varepsilon^2}\|\widetilde{f}_z(\theta_{\hat{x}},\cdot)\|_{C^1[\pi+\varepsilon,2\pi-\varepsilon]} \\
&\quad\le\frac{C(1+|z|)\|u^\infty(\hat{x},\cdot)\|_{C^1(\overline{\mathbb{S}^1_-})}}{R\varepsilon^2}\le\frac{C(1+|z|)}{R\varepsilon^2}. \qquad (3.30)
\end{aligned}
$$

Combining (3.29) and (3.30) and then taking $\varepsilon = R^{-1/3}$ give

$$
\int_0^\pi |\widetilde{w}_z(R,\theta_{\hat{x}})|\,d\theta_{\hat{x}}\le C\varepsilon+\frac{C(1+|z|)}{R\varepsilon^2}\le C\frac{1+|z|}{R^{1/3}}. \qquad (3.31)
$$

Now, define

$$
\widetilde{v}_z(R,\theta_{\hat{x}}):=\int_\pi^{2\pi} e^{2ikR\sin\theta_{\hat{x}}\sin\theta_d}\widetilde{g}_z(\theta_{\hat{x}},\theta_d)d\theta_d.
$$

Then it follows from Lemma 2.1 that

$$
\begin{aligned}
\int_0^\pi |\widetilde{v}_z(R,\theta_{\hat{x}})|d\theta_{\hat{x}} &= \int_{[\varepsilon,\pi-\varepsilon]}|\widetilde{v}_z(R,\theta_{\hat{x}})|d\theta_{\hat{x}}+\int_{[0,\varepsilon]\cup[\pi-\varepsilon,\pi]}|\widetilde{v}_z(R,\theta_{\hat{x}})|d\theta_{\hat{x}} \\
&\le C\varepsilon+\int_{[\varepsilon,\pi-\varepsilon]}|\widetilde{v}_z(R,\theta_{\hat{x}})|d\theta_{\hat{x}} \\
&\le C\varepsilon+\int_{[\varepsilon,\pi-\varepsilon]}\left|\int_{[\pi,3\pi/2-\varepsilon]\cup[3\pi/2+\varepsilon,2\pi]} e^{2ikR\sin\theta_{\hat{x}}\sin\theta_d}\widetilde{g}_z(\theta_{\hat{x}},\theta_d)d\theta_d\right|d\theta_{\hat{x}} \\
&\quad+\int_{[\varepsilon,\pi-\varepsilon]}\left|\int_{[3\pi/2-\varepsilon,3\pi/2+\varepsilon]} e^{2ikR\sin\theta_{\hat{x}}\sin\theta_d}\widetilde{g}_z(\theta_{\hat{x}},\theta_d)d\theta_d\right|d\theta_{\hat{x}} \\
&\le C\varepsilon+\int_{[\varepsilon,\pi-\varepsilon]}\left|\int_{[\pi,3\pi/2-\varepsilon]\cup[3\pi/2+\varepsilon,2\pi]} e^{2ikR\sin\theta_{\hat{x}}\sin\theta_{\theta_d}}\widetilde{g}_z(\theta_{\hat{x}},\theta_d)d\theta_d\right|d\theta_{\hat{x}}. \qquad (3.32)
\end{aligned}
$$

Let $v_{\theta_{\hat{x}}}(\theta_d)=4\varepsilon^{-2}\sin\theta_{\hat{x}}\sin\theta_d$. It is easy to see that $v'_{\theta_{\hat{x}}}(\theta_d)=4\varepsilon^{-2}\sin\theta_{\hat{x}}\cos\theta_d$, and thus we have that for $\theta_{\hat{x}}\in[\varepsilon,\pi-\varepsilon]$ and $\theta_d\in[\pi,3\pi/2-\varepsilon]\cup[3\pi/2+\varepsilon,2\pi]$,

$$
|v'_{\theta_{\hat{x}}}(\theta_d)|=\frac{4}{\varepsilon^2}|\sin\theta_{\hat{x}}||\cos\theta_d|=\frac{4}{\varepsilon^2}|\sin\theta_{\hat{x}}||\sin(\theta_d-3\pi/2)|\ge\frac{4}{\varepsilon^2}\sin\varepsilon\sin\varepsilon\ge\frac{4}{\varepsilon^2}\left(\frac{\varepsilon}{2}\right)^2=1
$$

and $v''_{\theta_{\hat{x}}}(\theta_d)=-4\varepsilon^{-2}\sin\theta_{\hat{x}}\sin\theta_d$ is monotone for $\theta_d\in[\pi,3\pi/2-\varepsilon]$ and for $\theta_d\in[3\pi/2+\varepsilon,2\pi]$.

Then, by Lemmas 2.1, 3.1, and 3.3 we find that for $\theta_{\hat{x}} \in [\varepsilon, \pi - \varepsilon]$,

$$\begin{aligned}
&\left| \int_{[\pi,3\pi/2-\varepsilon]\cup[3\pi/2+\varepsilon,2\pi]} e^{2ikR\sin\theta_{\hat{x}}\sin\theta_d} \widetilde{g}_z(\theta_{\hat{x}},\theta_d) d\theta_d \right| \\
&= \left| \int_{[\pi,3\pi/2-\varepsilon]\cup[3\pi/2+\varepsilon,2\pi]} e^{(ikR\varepsilon^2/2)v_{\theta_{\hat{x}}}(\theta_d)} \widetilde{g}_z(\theta_{\hat{x}},\theta_d) d\theta_d \right| \\
&\le \frac{C}{R\varepsilon^2} \|\widetilde{g}_z(\theta_{\hat{x}},\cdot)\|_{C^1([\pi,3\pi/2-\varepsilon]\cup[3\pi/2+\varepsilon,2\pi])} \\
&\le \frac{C(1+|z|)}{R\varepsilon^2} \|u^\infty(\hat{x},\cdot)\|_{C^1(\overline{S^1_-})} \le \frac{C(1+|z|)}{R\varepsilon^2}. \qquad (3.33)
\end{aligned}$$

Combining (3.32) and (3.33) and taking $\varepsilon = R^{-1/3}$ yield

$$\int_0^\pi |\widetilde{v}_z(R,\theta_{\hat{x}})| d\theta_{\hat{x}} \le C\varepsilon + \frac{C(1+|z|)}{R\varepsilon^2} \le C\frac{1+|z|}{R^{1/3}}. \qquad (3.34)$$

Finally, combining (3.27), (3.28), (3.31), and (3.34) gives

$$\begin{aligned}
&\sum_{i=1}^3 \left| \int_{\partial B_R^+} U_i(x,z)\overline{W_j(x,z)} dx \right| + \sum_{i=1}^4 \left| \int_{\partial B_R^+} W_i(x,z)\overline{W_j(x,z)} dx \right| \\
&\le C(1+|z|)\left(C\frac{1+|z|}{R^{1/3}} + \frac{C}{R} \right) \le C\frac{(1+|z|)^2}{R^{1/3}}, \quad j = 2,3.
\end{aligned}$$

The proof is thus completed. ∎

For $z \in \mathbb{R}^2$ define the function

$$F(R,z) := \int_{\partial B_R^+} |U(x,z)|^2 \, dx, \qquad (3.35)$$

where $U(x,z)$ is given in (3.2). The following lemma gives the properties of $F(R,z)$ for sufficiently large R. The proof of this lemma is mainly based on the method of stationary phase and will be presented in Appendix A.

Lemma 3.8. *For $z \in \mathbb{R}^2$ and $R > 0$ we have $F(R,z) = F_0(z) + F_{0,Res}(R,z)$, where*

$$F_0(z) := \int_{\mathbb{S}^1_+} \left| \int_{\mathbb{S}^1_-} u^\infty(\hat{x},d) e^{-ikz\cdot d} ds(d) - \left(\frac{2\pi}{k}\right)^{1/2} e^{-\frac{\pi}{4}i} \left(e^{-ik\hat{x}\cdot z'} + e^{-ik\hat{x}\cdot z} \right) \right|^2 ds(\hat{x}) \qquad (3.36)$$

which is independent on R, and $F_{0,Res}(R,z)$ satisfies the estimate

$$|F_{0,Res}(R,z)| \le C\frac{(1+|z|)^4}{R^{1/4}} \qquad (3.37)$$

for sufficiently large R. Here, $C > 0$ is a constant independent of R and z.

From (3.7) it follows that

$$I^{Phaseless}(z) = \int_{\partial B_R^+} |U(x,z)|^2 dx + 2\mathrm{Re} \int_{\partial B_R^+} U(x,z)\overline{W(x,z)} dx + \int_{\partial B_R^+} |W(x,z)|^2 dx.$$

Define

$$F_{Res}(R,z) := 2\mathrm{Re} \int_{\partial B_R^+} U(x,z)\overline{W(x,z)} dx + \int_{\partial B_R^+} |W(x,z)|^2 dx.$$

Then, by Lemmas 3.6, 3.7, and 3.8 we obtain the main theorem of this section.

Theorem 3.9. *For $z \in \mathbb{R}^2$ and $R > 0$ we have*

$$I^{Phaseless}(z) = F(R,z) + F_{Res}(R,z), \tag{3.38}$$

where $F(R,z)$ is defined in (3.35) and $F_{Res}(R,z)$ satisfies the estimate

$$|F_{Res}(R,z)| \le C\frac{(1+|z|)^2}{R^{1/3}} \tag{3.39}$$

for R large enough and $C > 0$ independent of R and z. Further, $F(R,z) = F_0(z) + F_{0,Res}(R,z)$, where $F_0(z)$ is defined in (3.36) and $F_{0,Res}(R,z)$ satisfies the estimate (3.37).

With the help of the above analysis, we now study properties of the imaging function $I^{Phaseless}(z)$, $z \in \mathbb{R}^2$. Let K be a bounded domain which contains the local perturbation Γ_p of the locally rough surface Γ. From Theorem 3.9 it is easy to see that if R is large enough, then $I^{Phaseless}(z) \approx F(R,z)$ for $z \in K$ with $F(R,z)$ given by (3.35). Thus the imaging function $I^{Phaseless}(z)$ is approximately equal to the function $F(R,z)$ for $z \in K$. Therefore, in what follows, we investigate the properties of the function $F(R,z)$. We will make use of the theory of scattering by unbounded rough surfaces. To this end, for $b \in \mathbb{R}$ let $U_b^+ = \{x = (x_1, x_2) \in \mathbb{R}^2 | x_2 > b\}$ and $\Gamma_b = \{x = (x_1, x_2) \in \mathbb{R}^2 | x_2 = b\}$. Further, let $BC(\Gamma)$ denote the Banach space of functions which are bounded and continuous on Γ with the norm $\|\psi\|_{\infty,\Gamma} := \sup_{x\in\Gamma} |\psi(x)|$ for $\psi \in BC(\Gamma)$. Then the problem of scattering by an unbounded, sound-soft, rough surface can be formulated as the following Dirichlet boundary value problem (see [10, 11, 53]).

Dirichlet problem (DP). Given $g \in BC(\Gamma)$, determine $u \in C^2(D_+) \cap C(\overline{D_+})$ such that

(i) u satisfies the Helmholtz equation (1.1);

(ii) $u = g$ on Γ;

(iii) for some $a \in \mathbb{R}$,

$$\sup_{x\in D_+} x_2^a |u(x)| < \infty; \tag{3.40}$$

(iv) u satisfies the upward propagating radiation condition (UPRC): for some $b > h_+ := \sup_{x_1\in\mathbb{R}} h(x_1)$ and $\phi \in L^\infty(\Gamma_b)$,

$$u(x) = 2\int_{\Gamma_b} \frac{\partial \Phi_k(x,y)}{\partial y_2} \phi(y) ds(y), \quad x \in U_b^+, \tag{3.41}$$

where $\Phi_k(x,y) := (i/4)H_0^{(1)}(k|x-y|), x, y \in \mathbb{R}^2, x \ne y$, is the free-space Green's function for the Helmholtz equation $\Delta u + k^2 u = 0$ in $\mathbb{R}^2$.

The well-posedness of the problem (DP) has been established in [10, 11, 53], using the integral equation method. The following theorem tells us that for arbitrarily fixed $z \in \mathbb{R}^2$ the function $U(x,z)$ given by (3.2) is the unique solution to the Dirichlet problem (DP) with the boundary data involving the Bessel function of order 0.

Theorem 3.10. *For arbitrarily fixed $z \in \mathbb{R}^2$, $U(x,z)$ given by (3.2) satisfies the Dirichlet problem* (DP) *with the boundary data*

$$g(x) = g_z(x) := -2\pi J_0(k|x-z|), \quad x \in \Gamma, \tag{3.42}$$

where J_0 is the Bessel function of order 0.

Proof. Arbitrarily fix $d \in \mathbb{S}^1_-$ and define $\widetilde{u}^s(x,d) := u^s(x,d) - e^{ikx\cdot d'}$ with $x \in D_+$. From the well-posedness of the scattering problem (1.1)–(1.5), it is easily seen that $\widetilde{u}^s(x,d)$ satisfies the Helmholtz equation (1.1) and the condition (3.40). Since $u^s(x,d)$ satisfies the Sommerfeld radiation condition (1.5), it follows from [9, Theorem 2.9] that $u^s(x,d)$ also satisfies the UPRC condition (3.41). Further, by [9, Remark 2.15] we know that $e^{ikx\cdot d'}$ satisfies the UPRC condition (3.41). As a result, $\widetilde{u}^s(x,d)$ satisfies the UPRC condition (3.41), and thus we apply the boundary condition (1.3) to deduce that $\widetilde{u}^s(x,d)$ is the solution to the Dirichlet problem (DP) with the boundary data $g(x) = -u^i(x,d) = -e^{ikx\cdot d}$. Furthermore, by the definition of $U(x,z)$ we see that

$$U(x,z) = \int_{\mathbb{S}^1_-} \left[\widetilde{u}^s(x,d)e^{-ikz\cdot d} - e^{ik(x\cdot d' - z'\cdot d)}\right] ds(d).$$

Then, by the Funk–Hecke formula (see, e.g., [57, Lemma 2.1]) it is derived that $U(x,z) = -2\pi J_0(k|x-z|)$, $x \in \Gamma$, and so, $U(x,z)$ satisfies the Dirichlet problem (DP) with the boundary data given by (3.42). The theorem is thus proved. ∎

Properties of solutions to the Dirichlet problem (DP) with the boundary data $g(x) = aJ_0(k|x-z|)$, $x \in \Gamma$, for any $a \in \mathbb{R}$ have been investigated in the case when Γ is a globally rough surface (see [37, section 3]). From the discussions in [37, section 3], it is expected that for any x in the compact subset of D_+ the function $U(x,z)$ given in (3.2) will take a large value when $z \in \Gamma$ and decay as z moves away from Γ. As a result, it is expected that for any fixed $R > 0$ the function $F(R,z)$ defined in (3.35) will take a large value when $z \in \Gamma$ and decay as z moves away from Γ. Thus, by Theorem 3.9 we know that for any bounded sampling region K the imaging function $I^{Phaseless}(z)$ will have similar properties as $F(R,z)$ with $z \in K$ if R is large enough, as seen in the numerical experiments presented in the next section.

Remark 3.11. In the numerical experiments, we measure the phaseless total-field data $|u(x^{(i)}, d^{(j)})|$, $i = 1,2,\ldots,M$, $j = 1,2,\ldots,N$, where $x^{(i)} = (x_1^{(i)}, x_2^{(i)})$ and $d^{(j)} = (d_1^{(j)}, d_2^{(j)})$ are uniformly distributed points on ∂B_R^+ and $\mathbb{S}^1_-$, respectively. Accordingly, the imaging function $I^{Phaseless}(z)$ is approximated as

$$I^{Phaseless}(z) \approx \frac{\pi^3 R}{MN^2}\sum_{i=1}^{M}\left|\sum_{j=1}^{N}\left[\left(\left|u(x^{(i)},d^{(j)})\right|^2-2+e^{2ikx_2^{(i)}d_2^{(j)}}\right)e^{ik(x^{(i)}-z)\cdot d^{(j)}}-e^{ik\left(x^{(i)\prime}-z'\right)\cdot d^{(j)}}\right]\right|^2, \tag{3.43}$$

where $x^{(i)\prime} := (x_1^{(i)}, -x_2^{(i)})$.

The direct imaging algorithm for our inverse problem can be given in the following algorithm.

Algorithm 3.1. *Let K be the sampling region which contains the local perturbation Γ_p of the locally rough surface Γ.*

(1) *Choose $\mathcal{T}_m$ to be a mesh of K and take R to be a large number.*
(2) *Collect the phaseless total-field data $\left|u(x^{(i)},d^{(j)})\right|$, $i=1,2,\ldots,M$, $j=1,2,\ldots,N$, with $x^{(i)}\in\partial B_R^+$ and $d^{(j)}\in\mathbb{S}_-^1$, generated by the incident plane waves $u^i(x,d^{(j)}) = e^{ikx\cdot d^{(j)}}$, $j=1,2,\ldots,N$.*
(3) *For all sampling points $z\in\mathcal{T}_m$, compute the imaging function $I^{Phaseless}(z)$ given in (3.43).*
(4) *Locate all those sampling points $z\in\mathcal{T}_m$ such that $I^{Phaseless}(z)$ takes a large value, which represent the part of the locally rough surface Γ in the sampling region K.*

Remark 3.12. Let K be the bounded sampling domain as above. From Lemma 3.8 it is seen that if R is large enough, then $F(R,z)\approx F_0(z)$ for $z\in K$, and so by the properties of $F(R,z)$ as discussed above we know that the function $F_0(z)$ defined in (3.36) will be expected to take a large value when $z\in\Gamma$ and decay as z moves away from Γ. Based on this, we define $I^{Full}(z) := F_0(z)$ for $z\in\mathbb{R}^2$ to be the imaging function with the full far-field data $u^\infty(\hat{x},d)$ with $\hat{x}\in\mathbb{S}_+^1$ and $d\in\mathbb{S}_-^1$. In the numerical experiments presented in the next section, we will show the imaging results of $I^{Full}(z)$ to compare with those of the imaging function $I^{Phaseless}(z)$. Therefore, we will take the full far-field measurement data $u^\infty(\hat{x}^{(i)},d^{(j)})$, $i=1,2,\ldots,L$, $j=1,2,\ldots,N$, where $\hat{x}^{(i)}$ and $d^{(j)}$ are uniformly distributed points on $\mathbb{S}_+^1$ and $\mathbb{S}_-^1$, respectively. Accordingly, the imaging function $I^{Full}(z)$ is approximated as

$$I^{Full}(z) \approx \frac{\pi}{L}\sum_{i=1}^{L}\left|\frac{\pi}{N}\left(\sum_{j=1}^{N}u^\infty(\hat{x}^{(i)},d^{(j)})e^{-ikz\cdot d^{(j)}}\right)-\left(\frac{2\pi}{k}\right)^{1/2}e^{-\pi i/4}\left(e^{-ik\hat{x}^{(i)}\cdot z'}+e^{-ik\hat{x}^{(i)}\cdot z}\right)\right|^2.$$

The direct imaging algorithm based on the imaging function $I^{Full}(z)$ can be given similarly as in Algorithm 3.1.

Remark 3.13. From (3.1) and (3.43) it is seen that the imaging function $I^{Phaseless}(z)$ of our direct imaging method uses integrals (or sums in the numerical approximation) with respect to the measurement data, which may serve as an excellent filter for white noise. Therefore, our direct imaging method based on the imaging function $I^{Phaseless}(z)$ should be very robust with respect to white noise in the data. This is indeed confirmed by the numerical experiments presented in the next section.

4. Numerical experiments. In this section, we present several numerical experiments to demonstrate the effectiveness of our imaging algorithm with the phaseless total-field data. Though the locally rough surface is assumed to be smooth in the above sections, we will also consider the reconstructed results for the case when the locally rough surface is piecewise smooth. In addition, in each example, we will also present imaging results of the imaging algorithm with full far-field data to compare the reconstruction results using both the phaseless near-field measurement data and the full far-field measurement data. To generate the synthetic data, we use the integral equation method proposed in [54] to solve the forward scattering problem (1.1)–(1.5). Further, the noisy phaseless near-field data $|u_\delta(x,d)|$, $x \in \partial B_R^+$, $d \in \mathbb{S}_-^1$, and the noisy full far-field data $u_\delta^\infty(\hat{x},d)$, $\hat{x} \in \mathbb{S}_+^1$, $d \in \mathbb{S}_-^1$, are simulated by

$$|u_\delta(x,d)| = |u(x,d)|\,(1+\delta\zeta_1)\,,$$
$$u_\delta^\infty(\hat{x},d) = u^\infty(\hat{x},d) + \delta\,(\zeta_2 + i\zeta_3)\,|u^\infty(\hat{x},d)|,$$

where δ is the noise ratio and $\zeta_1, \zeta_2, \zeta_3$ are the normally distributed random numbers in $[-1,1]$. The numerical examples below illustrate that our direct imaging algorithm is also very robust with respect to white noise in the data, which is consistent with our discussions in Remark 3.13.

In all the figures presented, we use a solid line to represent the actual curves.

Example 1. We first investigate the effect of the noise ratio δ on the imaging results. The locally rough surface is given by

$$h(x_1) = 0.1\phi\left(\frac{x_1+0.2}{0.3}\right) - 0.08\phi\left(\frac{x_1-0.3}{0.2}\right),$$

where

$$\phi(x) := \sum_{j=0}^{5} \frac{(-1)^j \binom{5}{j} \left(x+\frac{5}{2}-j\right)_+^4}{4!} \quad \text{with} \quad x_+^4 := \begin{cases} x^4, & x \geq 0, \\ 0, & x < 0, \end{cases}$$

is the cubic spline function. The wave number is set to be $k = 40$. We first consider the inverse problem with phaseless near-field data. We choose the radius of the measurement circle ∂B_R^+ to be $R = 4$ and the number of both the measurement points and the incident directions to be the same with $M = N = 200$. Figure 4.1 presents the imaging results of $I^{Phaseless}(z)$ from the measured phaseless near-field data without noise, with 10% noise, with 20% noise, and with 40% noise, respectively. Next, we consider the inverse problem with full far-field data. We choose the number of both the measured observation directions and the measured incident directions to be the same as well with $L = N = 100$. Figure 4.2 presents the imaging results of $I^{Full}(z)$ from the measured full far-field data without noise, with 10% noise, with 20% noise, and with 40% noise, respectively. As shown by Figures 4.1 and 4.2, the imaging results given by the imaging function $I^{Phaseless}(z)$ with phaseless near-field data are good though the imaging results of the imaging function $I^{Full}(z)$ with full far-field data are better than those of the imaging function $I^{Phaseless}(z)$ with phaseless near-field data.

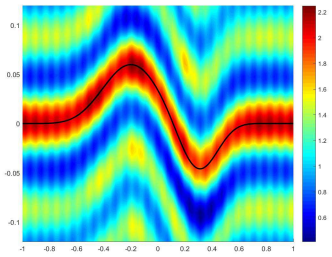

(a) **No noise, k=40, R=4**

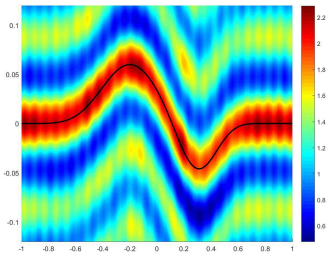

(b) **10% noise, k=40, R=4**

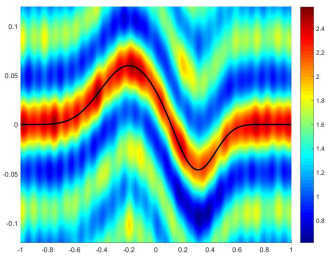

(c) **20% noise, k=40, R=4**

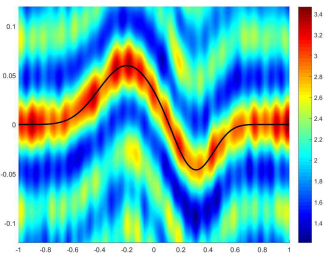

(d) **40% noise, k=40, R=4**

Figure 4.1. *Imaging results of* $I^{Phaseless}(z)$ *with measured phaseless near-field data, where the solid line represents the actual curve. The number of both the measured points and the incident directions is chosen to be the same with* $M = N = 200$.

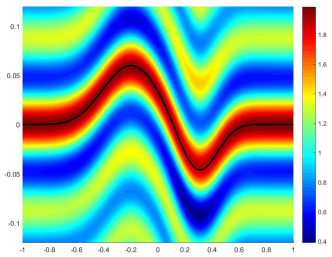

(a) **No noise, k=40**

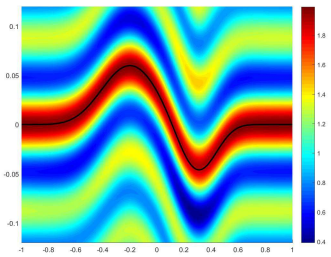

(b) **10% noise, k=40**

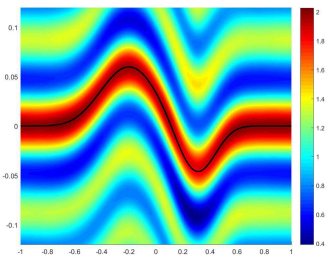

(c) **20% noise, k=40**

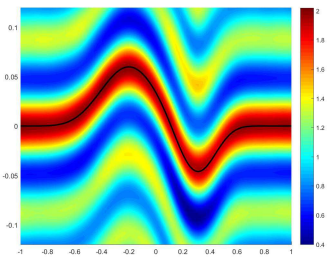

(d) **40% noise, k=40**

Figure 4.2. *Imaging results of* $I^{Full}(z)$ *with measured full far-field data, where the solid line represents the actual curve. The number of both the measured points and the incident directions is chosen to be the same with* $L = N = 100$.

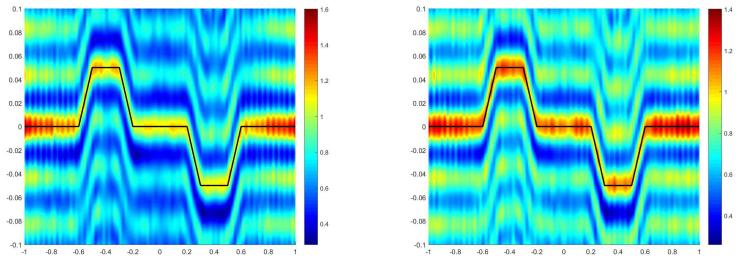

(a) **20% noise, k=80, R=1.2** (b) **20% noise, k=80, R=1.6**

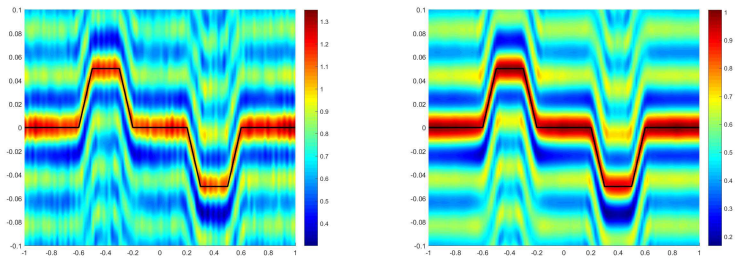

(c) **20% noise, k=80, R=2** (d) **20% noise, k=80**

Figure 4.3. (a)–(c) *Imaging results of* $I^{Phaseless}(z)$ *with the measured phaseless near-field data, where the number of the measurement points and the incident directions is chosen to be the same with* $M = N = 200$. (d) *Imaging result of* $I^{Full}(z)$ *with the measured full far-field data, where the number of the measurement points and the incident directions is chosen to be the same with* $L = N = 100$. *The solid line represents the actual curve.*

Example 2. We now consider the case when the local perturbation part of the boundary Γ is piecewise linear (the solid line in Figure 4.3). We choose the wave number to be $k = 80$ and the noise ratio to be $\delta = 20\%$. First consider the inverse problem with phaseless near-field data. For this case, we investigate the effect of the radius R of the measurement circle ∂B_R^+ on the imaging results. We choose the number of both the measurement points and the incident directions to be the same with $M = N = 200$. Figures 4.3(a)–4.3(c) present the imaging results of $I^{Phaseless}(z)$ with the measurement phaseless near-field data with the radius of the measurement circle ∂B_R^+ to be $R = 1.2, 1.6, 2$, respectively. From Figures 4.3(a)–4.3(c) it is seen that the reconstruction result is getting better with the radius of the measurement circle getting larger.

Second, we consider the inverse problem for full far-field data. We choose the numbers of measured directions and incident directions to be $L = N = 100$. Figure 4.3(d) presents the imaging results of I^{Full} from the measured full far-field data.

Example 3. We now consider the case of a multiscale surface profile given by

$$h(x_1) = \begin{cases} 0.3\exp\left[16/(25x_1^2 - 16)\right]\left[0.5 + 0.1\sin(16\pi x_1)\right]\sin(\pi x_1), & |x_1| < 4/5, \\ 0, & |x_1| \geq 4/5. \end{cases}$$

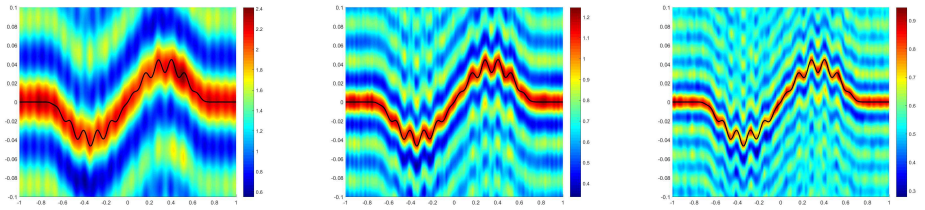

(a) **20% noise, k=40, R=4** (b) **20% noise, k=80, R=4** (c) **20% noise, k=120, R=4**

Figure 4.4. *The imaging results of $I^{Phaseless}(z)$ with the measurement phaseless near-field data. The number of the measurement points and the incident directions is chosen to be the same with $M = N = 400$. The solid line represents the actual curve.*

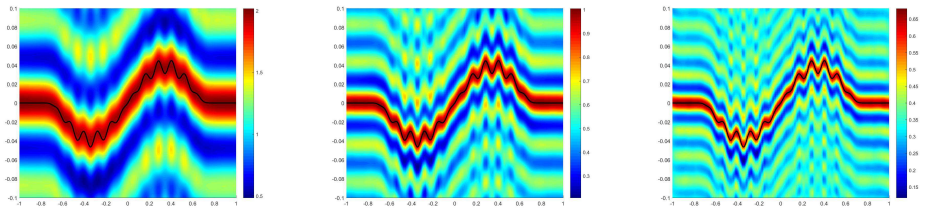

(a) **20% noise, k=40** (b) **20% noise, k=80** (c) **20% noise, k=120**

Figure 4.5. *The imaging results of $I^{Full}(z)$ with the measurement full far-field data, where the number of the measurement points and the incident directions is the same with $L = N = 100$. The solid line represents the actual curve.*

This profile consists of a macroscale represented by $0.15\exp[16/(25x_1^2 - 16)]\sin(\pi x_1)$ and a microscale represented by $0.03\exp[16/(25x_1^2 - 16)]\sin(16\pi x_1)\sin(\pi x_1)$. We will investigate the effect of the wave number k on the imaging results. The noise ratio is chosen to be $\delta = 20\%$. We first consider the inverse problem with phaseless near-field data. The radius of the measurement circle ∂B_R^+ is chosen to be $R = 4$ and the number of the measurement points and the incident directions is set to be $M = N = 400$. Figure 4.4 presents the imaging results of $I^{Phaseless}(z)$ with the measured phaseless near-field data with the wave number $k = 40, 80, 120$, respectively. Second, we consider the inverse problem with full far-field data. We choose the number of the measurement directions and the incident directions to be $L = N = 100$. Figure 4.5 shows the imaging results of $I^{Full}(z)$ with the measurement full far-field data with the wave number $k = 40, 80, 120$, respectively.

5. Conclusion. In this paper, we considered the inverse scattering problem by locally rough surfaces with phaseless near-field data. We have proved that the locally rough surface is uniquely determined by the phaseless near-field data, generated by a countably infinite number of incident plane waves and measured on an open domain above the locally rough surface. A direct imaging method has also been proposed to reconstruct the locally rough surface from phaseless near-field data generated by incident plane waves and measured on the upper part of a sufficiently large circle. The theoretical analysis of the imaging method has been given based on the method of stationary phase and the property of the scattering

solution. As a by-product of the theoretical analysis, a similar direct imaging method with full far-field data has also been given to reconstruct the locally rough surface and to compare with the imaging method with phaseless near-field data. As an ongoing project, we are currently trying to extend the results to the case of incident point sources. In the near future, we hope to consider the more challenging case of electromagnetic waves.

Appendix A. The method of stationary phase and proof of Lemma 3.8. In [45], the author developed an error theory for the method of stationary phase for integrals of the form

$$I(\gamma) = \int_a^b e^{i\gamma p(t)} q(t)\,dt, \tag{A.1}$$

where $a, b \in \mathbb{R}$, γ is a large real parameter, the function $p(t)$ is real, and $q(t)$ is either real or complex. In what follows, we will briefly present some useful results in [45] and use these results to prove Lemma 3.8. For a comprehensive discussion of the method of stationary phase, the reader is referred to [45].

A.1. Error theory for the method of stationary phase. We first present an error theory for the method of stationary phase given in [45]. Let $a, b \in \mathbb{R}$, let $p(t)$ be a real function, and let $q(t)$ be either a real or a complex function. Assume that $a, b, p(t), q(t)$ are independent of the positive parameter γ. They have the following properties:

(i) In (a, b), $p^{(m+1)}$ and $q^{(m)}(t)$ are continuous, m being a nonnegative integer, and $p'(t) > 0$.

(ii) As $t \to a$ from the right,

$$p(t) \sim p(a) + \sum_{s=0}^{\infty} p_s (t-a)^{s+\mu}, \quad q(t) \sim \sum_{s=0}^{\infty} q_s (t-a)^{s+\lambda-1}, \tag{A.2}$$

where the coefficients p_0 and q_0 are nonzero, and μ and λ are constants satisfying that

$$\mu > 0, \ (m+1)\mu + 1 > \mathrm{Re}(\lambda) > 0.$$

Moreover, the first of these expansions is differentiable $m+1$ times and the second m times.

(iii) $p(b) \equiv \lim_{t \to b-}\{p(t)\}$ is finite, and each of the functions

$$P_s(t) \equiv \left\{ \frac{1}{p'(t)} \frac{d}{dt} \right\}^s \frac{q(t)}{p'(t)}, \quad s = 0, 1, \ldots, m, \tag{A.3}$$

tends to a finite limit as $t \to b-$. In particular, (A.3) is satisfied if $p^{(m+1)}(t)$ and $q^{(m)}(t)$ are continuous at b and $p'(b) \neq 0$.

In consequence of condition (i) there is a one-to-one relationship between t and the variable v, defined by

$$v = p(t) - p(a). \tag{A.4}$$

In terms of this variable the integral (A.1) transforms into

$$\int_a^b e^{i\gamma p(t)} q(t)\,dt = e^{i\gamma p(a)} \int_0^{p(b)-p(a)} e^{i\gamma v} f(v)\,dv,$$

in which

$$f(v) = q(t)/p'(t) = P_0(t). \tag{A.5}$$

Again, condition (i) shows that $f(v)$ and its first m derivatives are continuous when $0 < v < p(b) - p(a)$. For small v, $f(v)$ can be expanded in asymptotic series of the form

$$f(v) \sim \sum_{s=0}^{\infty} a_s v^{(s+\lambda-\mu)/\mu}. \tag{A.6}$$

The coefficients a_s depend on p_s and q_s and may be found by standard procedures of reverting series. In particular,

$$a_0 = \frac{q_0}{\mu p_0^{\lambda/\mu}}, \quad a_1 = \left\{ \frac{q_1}{\mu} - \frac{(\lambda+1)p_1 q_0}{\mu^2 p_0} \right\} \frac{1}{p_0^{(\lambda+1)/\mu}}. \tag{A.7}$$

The following theorem gives an asymptotic expansion of the integral (A.1) with an error bound (see Theorem 1 and estimates (6.3) and (6.7) in [45]).

Theorem A.1 (Theorem 1 and estimates (6.3) and (6.7) in [45]). *Assume the conditions and notation of this section, and let n be a nonnegative integer satisfying*

$$m\mu - \lambda \le n < (m+1)\mu - \lambda + 1 \quad (\lambda \text{ real}) \tag{A.8}$$

or

$$m\mu - \mathrm{Re}(\lambda) < n < (m+1)\mu - \mathrm{Re}(\lambda) + 1 \quad (\lambda \text{ complex}). \tag{A.9}$$

If $p(b) < \infty$, then we have

$$\begin{aligned} \int_a^b e^{i\gamma p(t)} q(t)\,dt = {} & e^{i\gamma p(a)} \sum_{s=0}^{n-\nu} \exp\left\{ \frac{(s+\lambda)\pi i}{2\mu} \right\} \Gamma\left(\frac{s+\lambda}{\mu} \right) \frac{a_s}{\gamma^{(s+\lambda)/\mu}} \\ & - e^{i\gamma p(b)} \sum_{s=0}^{m-1} P_s(b) \left(\frac{i}{\gamma} \right)^{s+1} + \delta_{m,n}(\gamma) - \varepsilon_{m,n}(\gamma). \end{aligned} \tag{A.10}$$

Here, $\nu = 0$ when $n = m\mu - \lambda$, and $\nu = 1$ in all other cases. As usual, empty sums are understood to be zero. Further, the error terms $\delta_{m,n}$ and $\varepsilon_{m,n}$ satisfy

$$|\delta_{m,n}(\gamma)| \le [|Q_{m+1,n}(a)| + |Q_{m+1,n}(b)| + \mathcal{V}_{a,b}\{Q_{m+1,n}(t)\}]\,\gamma^{-m-1} \tag{A.11}$$

provided that the right-hand side is finite, and

$$|\varepsilon_{m,n}(\gamma)| \le \frac{2}{\gamma^{m+1}} \sum_{s=0}^{n-1} \frac{\Gamma\{(s+\lambda)/\mu\}}{|\Gamma\{(s+\lambda-m\mu)/\mu\}|} \frac{|a_s|}{\{p(b)-p(a)\}^{(m\mu+\mu-s-\lambda)/\mu}}. \tag{A.12}$$

Here, $Q_{m+1,n}$ is given by

$$Q_{m+1,n}(t) = P_m(t) - \sum_{s=0}^{n-1} \frac{\Gamma\{(s+\lambda)/\mu\}}{\Gamma\{[s+\lambda+\mu-(m+1)\mu]/\mu\}} \frac{a_s}{\{p(t)-p(a)\}^{[(m+1)\mu-s-\lambda]/\mu}}, \tag{A.13}$$

and $\mathscr{V}_{a,b}\{Q_{m+1,n}(t)\}$ denotes the total variation of the function $Q_{m+1,n}(t)$ which is given by

$$\mathscr{V}_{a,b}\{Q_{m+1,n}(t)\} = \int_a^b |Q'_{m+1,n}(t)|dt.$$

A.2. Proof of Lemma 3.8. In this section, we prove Lemma 3.8, employing Theorem A.1. To do this, we need to estimate the function U_i, $i = 1, 2, 3$, defined in (3.4)–(3.6).

Lemma A.2. *Let $x \in D_+$ and $z \in \mathbb{R}^2$. Then we have*

$$U_1(x,z) = \frac{e^{ik|x|}}{|x|^{1/2}} \int_{\mathbb{S}^1_-} u^\infty(\hat{x},d) e^{-ikz\cdot d} ds(d) + U_{1,Res}(x,z) \tag{A.14}$$

with

$$|U_{1,Res}(x,z)| \le \frac{C}{|x|^{3/2}} \quad as \ \ |x| \to +\infty, \tag{A.15}$$

where $C > 0$ is a constant independent of x and z.

Proof. Multiply (2.1) by $e^{-ikz\cdot d}$ and integrate with respect to d over $\mathbb{S}^1_-$ to obtain (A.14) with $U_{1,Res}$ being given by

$$U_{1,Res}(x,z) := \int_{\mathbb{S}^1_-} u^s_{Res}(x,d) e^{-ikz\cdot d} ds(d).$$

The inequality (A.15) then follows from (2.3). The lemma is thus proved. ∎

Lemma A.3. *Let $x \in \mathbb{R}^2_+$ and $z \in \mathbb{R}^2$. Write $\hat{x} = x/|x| = (\cos\theta_{\hat{x}}, \sin\theta_{\hat{x}})$ with $\theta_{\hat{x}} \in (0,\pi)$. Then we have that for $\theta_{\hat{x}} \in (0,\pi)$,*

$$U_2(x,z) = -\frac{e^{ik|x|}}{|x|^{1/2}} e^{-\frac{\pi}{4}i} \left(\frac{2\pi}{k}\right)^{1/2} e^{-ik\hat{x}\cdot z'} + U_{2,Res}(x,z), \tag{A.16}$$

$$U_3(x,z) = -\frac{e^{ik|x|}}{|x|^{1/2}} e^{-\frac{\pi}{4}i} \left(\frac{2\pi}{k}\right)^{1/2} e^{-ik\hat{x}\cdot z} + U_{3,Res}(x,z), \tag{A.17}$$

where

$$|U_{j,Res}(x,z)| \le C\left(|z| + \frac{1}{|\sin\frac{\theta_{\hat{x}}}{2}|} + \frac{1}{|\sin\frac{\pi-\theta_{\hat{x}}}{2}|} + \frac{1}{|\sin\theta_{\hat{x}}|} + \int_0^{\theta_{\hat{x}}} \frac{(1+|z|)^3 t^2}{\sin^2 t} dt \right.$$
$$\left. + \int_0^{\pi-\theta_{\hat{x}}} \frac{(1+|z|)^3 t^2}{\sin^2 t} dt \right) \frac{1}{|x|}, \quad j = 2, 3, \tag{A.18}$$

for large $|x|$. Here, $C > 0$ is a constant independent of x and z.

Proof. We only consider the case for $U_2(x,z)$. The case for $U_3(x,z)$ can be proved similarly.

For $d \in \mathbb{S}^1_-$ and $z \in \mathbb{R}^2$, let $\theta_d, \theta_{\hat{z}}$ be the real numbers as defined at the end of section 1. Then we have

$$U_2(x,z) = -\int_{\mathbb{S}^1_-} e^{ik(x\cdot d' - z\cdot d)} ds(d) = -\int_{\pi}^{2\pi} e^{ik|x|\cos(\theta_d+\theta_{\hat{x}})} e^{-ik|z|\cos(\theta_d-\theta_{\hat{z}})} d\theta_d.$$

A straightforward calculation gives

$$\begin{aligned} -\overline{U_2(x,z)} &= \int_{\pi}^{2\pi-\theta_{\hat{x}}} e^{-ik|x|\cos(\theta_d+\theta_{\hat{x}})} e^{ik|z|\cos(\theta_d-\theta_{\hat{z}})} d\theta_d \\ &\quad + \int_{2\pi-\theta_{\hat{x}}}^{2\pi} e^{-ik|x|\cos(\theta_d+\theta_{\hat{x}})} e^{ik|z|\cos(\theta_d-\theta_{\hat{z}})} d\theta_d \\ &= \int_0^{\pi-\theta_{\hat{x}}} e^{-ik|x|\cos t} e^{ik|z|\cos(t+\theta_{\hat{x}}+\theta_{\hat{z}})} dt + \int_0^{\theta_{\hat{x}}} e^{-ik|x|\cos t} e^{ik|z|\cos(t-\theta_{\hat{x}}-\theta_{\hat{z}})} dt \\ &:= I_1(x,z) + I_2(x,z). \end{aligned} \tag{A.19}$$

We first estimate $I_1(x,z)$. Let $\gamma = |x|, a = 0, b = \pi - \theta_{\hat{x}}$, $p(t) = -k\cos t$, and $q(t) = e^{ik|z|\cos(t+\theta_{\hat{x}}+\theta_{\hat{z}})}$. Then it is easy to verify that $a, b, p(t), q(t)$ satisfy the assumptions in section A.1. In particular, $p(t), q(t)$ satisfy assumption (A.2) with $\mu = 2, \lambda = 1, p_0 = k/2$, and $q_0 = e^{ik|z|\cos(\theta_{\hat{x}}+\theta_{\hat{z}})}$, and the function P_0 defined in (A.3) is given by

$$P_0(t) = q(t)/p'(t) = e^{ik|z|\cos(t+\theta_{\hat{x}}+\theta_{\hat{z}})}/(k\sin t). \tag{A.20}$$

Let the relationship between t and v be given by (A.4) and let $f(v)$ be the function defined in (A.5). Then $f(v)$ has the form (A.6). In particular, it follows from (A.7) that the coefficient $a_0 = q_0/(\mu p_0^{\lambda/\mu}) = e^{ik|z|\cos(\theta_{\hat{x}}+\theta_{\hat{z}})}/(2k)^{1/2}$.

Choose $m = 0, n = 1$. Then m, n satisfy the condition (A.8). Thus it follows from (A.10) that

$$\begin{aligned} I_1(x,z) &= \int_a^b e^{i|x|p(t)} q(t) dt = e^{i|x|p(0)} exp\left\{\frac{\lambda\pi i}{2\mu}\right\} \Gamma\left(\frac{\lambda}{\mu}\right) \frac{a_0}{|x|^{\lambda/\mu}} + \delta_{0,1}(|x|) - \varepsilon_{0,1}(|x|) \\ &= \frac{e^{-ik|x|}}{|x|^{1/2}} e^{\pi i/4} \left(\frac{\pi}{2k}\right)^{1/2} e^{ik|z|\cos(\theta_{\hat{x}}+\theta_{\hat{z}})} + \delta_{0,1}(|x|) - \varepsilon_{0,1}(|x|) \\ &= \frac{e^{-ik|x|}}{|x|^{1/2}} e^{\pi i/4} \left(\frac{\pi}{2k}\right)^{1/2} e^{ik\hat{x}\cdot z'} + \delta_{0,1}(|x|) - \varepsilon_{0,1}(|x|). \end{aligned} \tag{A.21}$$

Further, by (A.13) and (A.20) we have

$$\begin{aligned} Q_{1,1}(t) &= P_0(t) - \frac{a_0}{(p(t)-p(a))^{1/2}} \\ &= \frac{1}{k\sin t}\left(e^{ik|z|\cos(t+\theta_{\hat{x}}+\theta_{\hat{z}})} - e^{ik|z|\cos(\theta_{\hat{x}}+\theta_{\hat{z}})}\cos\frac{t}{2}\right) \end{aligned}$$

for $t \in (0, \pi - \theta_{\hat{x}})$. It is easy to see that

$$|Q_{1,1}(0)| \le |z|, \quad |Q_{1,1}(\pi-\theta_{\hat{x}})| \le \frac{2}{k|\sin(\pi-\theta_{\hat{x}})|} = \frac{2}{k|\sin\theta_{\hat{x}}|} \tag{A.22}$$

and

$$Q'_{1,1}(t) = \frac{\left(\frac{1}{2}\sin\frac{t}{2}\sin t + \cos\frac{t}{2}\cos t\right) e^{ik|z|\cos(\theta_{\hat{x}}+\theta_{\hat{z}})}}{k\sin^2 t} - \frac{(ik|z|\sin(t+\theta_{\hat{x}}+\theta_{\hat{z}})\sin t + \cos t)\, e^{ik|z|\cos(t+\theta_{\hat{x}}+\theta_{\hat{z}})}}{k\sin^2 t} := \frac{h(t)}{k\sin^2 t}.$$

By a straightforward calculation, it is derived that

$$h(0) = h'(0) = 0 \quad |h''(t)| \le C(1+|z|)^3, \quad t \in \mathbb{R}.$$

Then, by the Taylor expansion we obtain that for $t \in (0, \pi - \theta_{\hat{x}})$,

$$|Q'_{1,1}(t)| \le C\frac{(1+|z|)^3 t^2}{\sin^2 t}. \tag{A.23}$$

Combining (A.11), (A.22), and (A.23) gives

$$\begin{aligned} |\delta_{0,1}(|x|)| &\le [|Q_{1,1}(0)| + |Q_{1,1}(\pi-\theta_{\hat{x}})| + \mathscr{V}_{0,\pi-\theta_{\hat{x}}}\{Q_{1,1}(t)\}]\,|x|^{-1} \\ &\le C\left(|z| + \frac{1}{|\sin\theta_{\hat{x}}|} + \int_0^{\pi-\theta_{\hat{x}}} \frac{(1+|z|)^3 t^2}{\sin^2 t}dt\right)\frac{1}{|x|}. \end{aligned} \tag{A.24}$$

Further, it follows from (A.12) that

$$|\varepsilon_{0,1}| \le \frac{2}{|x|}\frac{|a_0|}{(p(b)-p(a))^{1/2}} = \frac{1}{k|x|}\frac{1}{\left|\sin\frac{\pi-\theta_{\hat{x}}}{2}\right|}. \tag{A.25}$$

Let $I_{1,Res}(x,z) := \delta_{0,1}(|x|) - \varepsilon_{0,1}(|x|)$. Then combining (A.21), (A.24), and (A.25) yields

$$I_1(x,z) = \frac{e^{-ik|x|}}{|x|^{1/2}} e^{\pi i/4}\left(\frac{\pi}{2k}\right)^{1/2} e^{ik\hat{x}\cdot z'} + I_{1,Res}(x,z) \tag{A.26}$$

with

$$|I_{1,Res}(x,z)| \le C\left(|z| + \frac{1}{|\sin\frac{\pi-\theta_{\hat{x}}}{2}|} + \frac{1}{|\sin\theta_{\hat{x}}|} + \int_0^{\pi-\theta_{\hat{x}}} \frac{(1+|z|)^3 t^2}{\sin^2 t}dt\right)\frac{1}{|x|}. \tag{A.27}$$

Similarly, for $I_2(x,z)$ we have

$$I_2(x,z) = \frac{e^{-ik|x|}}{|x|^{1/2}} e^{\pi i/4}\left(\frac{\pi}{2k}\right)^{1/2} e^{ik\hat{x}\cdot z'} + I_{2,Res}(x,z), \tag{A.28}$$

where

$$|I_{2,Res}(x,z)| \le C\left(|z| + \frac{1}{|\sin\frac{\theta_{\hat{x}}}{2}|} + \frac{1}{|\sin\theta_{\hat{x}}|} + \int_0^{\theta_{\hat{x}}} \frac{(1+|z|)^3 t^2}{\sin^2 t}dt\right)\frac{1}{|x|}. \tag{A.29}$$

Now, let $U_{2,Res}(x,z) := -(\overline{I_{1,Res}(x,z)} + \overline{I_{2,Res}(x,z)})$. Then (A.16) with the estimate (A.18) follows from (A.19), (A.26), (A.27), (A.28), and (A.29). The proof is thus complete. ∎

Lemma A.4. *Let $z \in \mathbb{R}^2$ and let $U_{j,Res}(x,z), j = 2,3$, be the functions defined in Lemma A.3. Assume that $\delta > 0$ is small enough and $R > 0$ is large enough. Then, for any $x = R(\cos\theta_{\hat{x}}, \sin\theta_{\hat{x}})$ with $\theta_{\hat{x}} \in [\delta, \pi - \delta]$ we have*

$$|U_{j,Res}(x,z)| \le C\frac{(1+|z|)^3}{R\delta}, \quad j = 2,3, \tag{A.30}$$

where $C > 0$ is a constant independent of x and z.

Proof. For $\theta_{\hat{x}} \in [\delta, \pi - \delta]$ with δ small enough we have

$$\frac{1}{\left|\sin\frac{\theta_{\hat{x}}}{2}\right|} + \frac{1}{\left|\sin\frac{\pi-\theta_{\hat{x}}}{2}\right|} + \frac{1}{|\sin\theta_{\hat{x}}|} \le \frac{C}{\delta}$$

and

$$\begin{aligned}
&\int_0^{\theta_{\hat{x}}} \frac{(1+|z|)^3 t^2}{\sin^2 t}dt + \int_0^{\pi-\theta_{\hat{x}}} \frac{(1+|z|)^3 t^2}{\sin^2 t}dt \\
&\quad \le 2\int_0^{\pi-\delta} \frac{(1+|z|)^3 t^2}{\sin^2 t}dt \le C(1+|z|)^3\left(1 + \int_{\pi/2}^{\pi-\delta} \frac{1}{\sin^2 t}dt\right) \\
&\quad = C(1+|z|)^3\left(1 + \int_{\delta}^{\pi/2} \frac{1}{\sin^2 t}dt\right) \le C\frac{(1+|z|)^3}{\delta}.
\end{aligned}$$

This, together with Lemma A.3, implies the inequality (A.30). The proof is thus complete. ∎

We are now ready to prove Lemma 3.8.

Proof of Lemma 3.8. For arbitrarily fixed $z \in \mathbb{R}^2$, let $\delta = R^{-1/4}$ with $R > 0$ large enough. Define $\partial B^+_{R,\delta} := \{x = R(\cos\theta_{\hat{x}}, \sin\theta_{\hat{x}}) \mid \theta_{\hat{x}} \in (0,\delta) \cup (\pi - \delta, \pi)\}$ and define

$$\begin{aligned}
U_0(x,z) := \frac{e^{ik|x|}}{|x|^{1/2}}\Bigg[&\int_{\mathbb{S}^1_-} u^\infty(\hat{x},d)e^{-ikz\cdot d}ds(d) \\
&- \left(\frac{2\pi}{k}\right)^{1/2} e^{-\pi i/4}(e^{-ik\hat{x}\cdot z'} + e^{-ik\hat{x}\cdot z})\Bigg],
\end{aligned} \tag{A.31}$$

$$U_{Res}(x,z) := \sum_{j=1}^{3} U_{j,Res}(x,z), \tag{A.32}$$

where $U_{j,Res}(x,z), j = 1,2,3$, are given in (A.14), (A.16), and (A.17), respectively. Then it follows from Lemmas A.2 and A.3 that $U(x,z) = U_0(x,z) + U_{Res}(x,z)$. Now, by the definition of $U_0(x,z)$ and $U(x,z)$ and using Lemmas 2.1 and 3.4 we get

$$|U_0(x,z)| \le C\frac{1}{R^{1/2}}, \quad |U(x,z)| \le C\frac{1+|z|}{R^{1/2}} \quad \forall x \in \partial B^+_R, \tag{A.33}$$

which yields

$$|U_{Res}(x,z)| \le C\frac{1+|z|}{R^{1/2}} \quad \forall x \in \partial B_R^+. \tag{A.34}$$

On the other hand, by Lemmas A.2 and A.4 and on noting that $\delta = R^{-1/4}$ it follows that

$$|U_{Res}(x,z)| \le C_1\left(\frac{1}{R^{3/2}} + \frac{(1+|z|)^3}{\delta R}\right) \le C\frac{(1+|z|)^3}{R^{3/4}} \quad \forall x \in \partial B_R^+ \backslash \partial B_{R,\delta}^+. \tag{A.35}$$

We now prove (3.37) for the function $F_{0,Res}(x,z)$ defined in Lemma 3.8. Since $F(R,z) = F_0(z) + F_{0,Res}(R,z)$, and by the definition of $F(R,z)$, $F_0(z)$, and $U_0(x,z)$ (see (3.35), (3.36), and (A.31)), we have

$$\begin{aligned}
&\int_{\partial B_R^+} |U(x,z)|^2 dx \\
&= \int_{\mathbb{S}_+^1} \left| \int_{\mathbb{S}_-^1} u^\infty(x,d) e^{-ikz\cdot d} ds(d) - \left(\frac{2\pi}{k}\right)^{1/2} e^{-\pi i/4}\left(e^{-ik\hat{x}\cdot z'} + e^{-ik\hat{x}\cdot z}\right)\right|^2 ds(\hat{x}) \\
&\quad + F_{0,Res}(R,z) = \int_{\partial B_R^+} |U_0(x,z)|^2 dx + F_{0,Res}(R,z).
\end{aligned}$$

Thus we have

$$F_{0,Res}(x,z) = \int_{\partial B_R^+} U_0(x,z)\overline{U_{Res}(x,z)}dx + \int_{\partial B_R^+} U_{Res}(x,z)\overline{U(x,z)}dx. \tag{A.36}$$

From (A.33), (A.34), and (A.35) it follows that

$$\begin{aligned}
&\left|\int_{\partial B_R^+} U_0(x,z)\overline{U_{Res}(x,z)}dx\right| \\
&\quad \le \left|\int_{\partial B_{R,\delta}^+} U_0(x,z)\overline{U_{Res}(x,z)}dx\right| + \left|\int_{\partial B_R^+\backslash\partial B_{R,\delta}^+} U_0(x,z)\overline{U_{Res}(x,z)}dx\right| \\
&\quad \le CR\delta\frac{1}{R^{1/2}}\frac{1+|z|}{R^{1/2}} + CR\frac{1}{R^{1/2}}\frac{(1+|z|)^3}{\delta R} \\
&\quad = C\left((1+|z|)\delta + \frac{(1+|z|)^3}{\delta R^{1/2}}\right)
\end{aligned} \tag{A.37}$$

and

$$\begin{aligned}
&\left|\int_{\partial B_R^+} U_{Res}(x,z)\overline{U(x,z)}dx\right| \\
&\quad \le \left|\int_{\partial B_{R,\delta}^+} U_{Res}(x,y)\overline{U(x,z)}dx\right| + \left|\int_{\partial B_R^+\backslash\partial B_{R,\delta}^+} U_{Res}(x,z)\overline{U(x,z)}dx\right| \\
&\quad \le CR\delta\frac{1+|z|}{R^{1/2}}\frac{1+|z|}{R^{1/2}} + CR\frac{(1+|z|)^3}{\delta R}\frac{1+|z|}{R^{1/2}} \\
&\quad = C\left((1+|z|)^2\delta + \frac{(1+|z|)^4}{\delta R^{1/2}}\right).
\end{aligned} \tag{A.38}$$

Combining (A.36), (A.37), and (A.38) gives

$$|F_{0,Res}(R,z)| \le C\left((1+|z|)^2\delta + \frac{(1+|z|)^4}{\delta R^{1/2}}\right).$$

This, combined with the fact that $\delta = R^{-1/4}$, yields (3.37). Lemma 3.8 is thus proved. ∎

Acknowledgment. We thank the reviewers for the constructive comments.

REFERENCES

[1] H. Ammari, Y.T. Chow, and J. Zou, *Phased and phaseless domain reconstructions in the invere scattering problem via scattering coeffieicents*, SIAM J. Appl. Math., 76 (2016), pp. 1000–1030.
[2] T.M. Apostol, *Modular Functions and Dirichlet Series in Number Theory*, 2nd ed., Springer, New York, 1990.
[3] G. Bao, J. Gao, and P. Li, *Analysis of direct and inverse cavity scattering problems*, Numer. Math. Theory Methods Appl., 4 (2011), pp. 419–442.
[4] G. Bao, P. Li, and J. Lv, *Numerical solution of an inverse diffraction grating problem from phaseless data*, J. Opt. Soc. Amer. A, 30 (2013), pp. 293–299.
[5] G. Bao and J. Lin, *Imaging of local surface displacement on an infinite ground plane: The multiple frequency case*, SIAM J. Appl. Math., 71 (2011), pp. 1733–1752.
[6] G. Bao, P. Li, J. Lin, and F. Triki, *Inverse scattering problems with multi-frequencies*, Inverse Problems, 31 (2015), 093001.
[7] G. Bao and L. Zhang, *Shape reconstruction of the multi-scale rough surface from multi-frequency phaseless data*, Inverse Problems, 32 (2016), 085002.
[8] C. Burkard and R. Potthast, *A multi-section approach for rough surface reconstruction via the Kirsch–Kress scheme*, Inverse Problems, 26 (2010), 045007.
[9] S.N. Chandler-Wilde and B. Zhang, *Electromagnetic scattering by an inhomogeneous conducting or dielectric layer on a perfectly conducting plate*, Proc. A, 454 (1998), pp. 519–542.
[10] S.N. Chandler-Widle and B. Zhang, *A uniqueness result for scattering by infinite rough surfaces*, SIAM J. Appl. Math., 58 (1998), pp. 1774–1790.
[11] S.N. Chandler-Wilde, C.R. Ross, and B. Zhang, *Scattering by infinite one-dimensional rough surfaces*, Proc. A, 455 (1999), pp. 3767–3787.
[12] S.N. Chandler-Wilde and C. Lines, *A time domain point source method for inverse scattering by rough surfaces*, Computing, 75 (2005), pp. 157–180.
[13] X. Chen, *Computational Methods for Electromagnetic Inverse Scattering*, Wiley, New York, 2018.
[14] Z. Chen and G. Huang, *Phaseless imaging by reverse time migration: Acoustic waves*, Numer. Math. Theory Methods Appl., 10 (2017), pp. 1–21.
[15] Z. Chen and G. Huang, *A direct imaging method for electromagnetic scattering data without phase information*, SIAM J. Imaging Sci., 9 (2016), pp. 1273–1297.
[16] Z. Chen, S. Fang, and G. Huang, *A direct imaging method for the half-space inverse scattering problem with phaseless data*, Inverse Probl. Imaging, 11 (2017), pp. 901–916.
[17] R. Coifman, M. Goldberg, T. Hrycak, M. Israeli, and V. Rokhlin, *An improved operator expansion algorithm for direct and inverse scattering computations*, Waves Random Media, 9 (1999), pp. 441–457.
[18] D. Colton and R. Kress, *Inverse Acoustic and Electromagnetic Scattering Theory*, 3rd ed., Springer, New York, 2013.
[19] J.A. DeSanto and R.J. Wombell, *Reconstruction of rough surface profiles with the Kirchhoff approximation*, J. Opt. Soc. Amer. A, 8 (1991), pp. 1892–1897.
[20] J.A. DeSanto and R.J. Wombell, *The reconstruction of shallow rough-surface profiles from scattered field data*, Inverse Problems, 7 (1991), pp. L7–L12.
[21] M. Ding, J. Li, K. Liu, and J. Yang, *Imaging of local rough surfaces by the linear sampling method with near-field data*, SIAM J. Imaging Sci., 10 (2017), pp. 1579–1602.

[22] O. Ivanyshyn, *Shape reconstruction of acoustic obstacles from the modulus of the far field pattern*, Inverse Probl. Imaging, 1 (2007), pp. 609–622.
[23] O. Ivanyshyn and R. Kress, *Identification of sound-soft 3D obstacles from phaseless data*, Inverse Probl. Imaging, 4 (2010), pp. 131–149.
[24] O. Ivanyshyn and R. Kress, *Inverse scattering for surface impedance from phaseless far field data*, J. Comput. Phys., 230 (2011), pp. 3443–3452.
[25] X. Ji, X. Liu, and B. Zhang, *Target Reconstruction with a Reference Point Scatterer Using Phaseless Far Field Patterns*, preprint, arXiv:1805.08035v3, 2018.
[26] M.V. Klibanov, *Phaseless inverse scattering problems in three dimensions*, SIAM J. Appl. Math., 74 (2014), pp. 392–410.
[27] M.V. Klibanov, *A phaseless inverse scattering problem for the 3-D Helmholtz equation*, Inverse Probl. Imaging, 11 (2017), pp. 263–276.
[28] M.V. Klibanov and V.G. Romanov, *Reconstruction procedures for two inverse scattering problems without the phase information*, SIAM J. Appl. Math., 76 (2016), pp. 178–196.
[29] M.V. Klibanov and V.G. Romanov, *Uniqueness of a 3-D coefficient inverse scattering problem without the phase information*, Inverse Problems, 33 (2017), 095007.
[30] R. Kress and W. Rundell, *Inverse obstacle scattering with modulus of the far field pattern as data*, in Inverse Problems in Medical Imaging and Nondestructive Testing, H. Engl, A.K. Louis, and W. Rundell, eds., Springer, New York, 1997, pp. 75–92.
[31] R. Kress and T. Tran, *Inverse scattering for a locally perturbed half-plane*, Inverse Problems, 16 (2000), pp. 1541–1559.
[32] J. Li and H. Liu, *Recovering a polyhedral obstacle by a few backscattering measurements*, J. Differential Equations, 259 (2015), pp. 2101–2120.
[33] J. Li, H. Liu, and Y. Wang, *Recovering an electromagnetic obstacle by a few phaseless backscattering measurements*, Inverse Problems, 33 (2017), 035001.
[34] J. Li, H. Liu, and J. Zou, *Strengthened linear sampling method with a reference ball*, SIAM J. Sci. Comput., 31 (2010), pp. 4013–4040.
[35] P. Li, *An inverse cavity problem for Maxwell's equations*, J. Differential Equations, 252 (2012), pp. 3209–3225.
[36] J. Li, G. Sun, and B. Zhang, *The Kirsch-Kress method for inverse scattering by infinite locally rough interfaces*, Appl. Anal., 96 (2017), pp. 85–107.
[37] X. Liu, B. Zhang, and H. Zhang, *A direct imaging method for inverse scattering by an unbounded rough surface*, SIAM J. Imaging Sci., 11 (2018), pp. 1629–1650.
[38] J. Liu and J. Seo, *On stability for a translated obstacle with impedance boundary condition*, Nonlinear Anal., 59 (2004), pp. 731–744.
[39] X. Liu and B. Zhang, *Unique determination of a sound-soft ball by the modulus of a single far field datum*, J. Math. Anal. Appl., 365 (2010), pp. 619–624.
[40] A. Majda, *High frequency asymptotics for the scattering matrix and the inverse problem of acoustical scattering*, Commun. Pure Appl. Math., 29 (1976), pp. 261–291.
[41] S. Maretzke and T. Hohage, *Stability estimates for linearized near-field phase retrieval in X-ray phase contrast imaging*, SIAM J. Appl. Math., 77 (2017), pp. 384–408.
[42] A. Novikov, M. Moscoso, and G. Papanicolaou, *Illumination strategies for intensity-only imaging*, SIAM J. Imaging Sci., 8 (2015), pp. 1547–1573.
[43] R.G. Novikov, *Formulas for phase recovering from phaseless scattering data at a fixed frequency*, Bull. Sci. Math., 139 (2015), pp. 923–936.
[44] R.G. Novikov, *Explicit formulas and global uniqueness for phaseless inverse scattering in multidimensions*, J. Geom. Anal., 26 (2016), pp. 346–359.
[45] F.W.J. Olver, *Error bounds for stationary phase approximations*, SIAM J. Math. Anal., 5 (1974), pp. 19–29.
[46] L. Pan, Y. Zhong, X. Chen, and S.P. Yeo, *Subspace-based optimization method for inverse scattering problems utilizing phaseless data*, IEEE Trans. Geosci. Remote Sensing, 49 (2011), pp. 981–987.
[47] J. Shin, *Inverse obstacle backscattering problems with phaseless data*, Euro. J. Appl. Math., 27 (2016), pp. 111–130.

[48] M. Spivack, *Direct solution of the inverse problem for rough scattering at grazing incidence*, J. Phys. A Math. Gen., 25 (1992), pp. 3295–3302.
[49] Z. Wei, W. Chen, C. Qiu, and X. Chen, *Conjugate gradient method for phase retrieval based on Wirtinger derivative*, J. Opt. Soc. Amer. A, 34 (2017), pp. 708–712.
[50] A. Willers, *The Helmholtz equation in disturbed half-spaces*, Math. Methods Appl. Sci., 9 (1987), pp. 312–323.
[51] X. Xu, B. Zhang, and H. Zhang, *Uniqueness in inverse scattering problems with phaseless far-field data at a fixed frequency*, SIAM J. Appl. Math., 78 (2018), pp. 1737–1753.
[52] X. Xu, B. Zhang, and H. Zhang, *Uniqueness in inverse scattering problems with phaseless far-field data at a fixed frequency.* II, SIAM J. Appl. Math., 78 (2018), pp. 3024–3039.
[53] B. Zhang and S.N. Chandler-Wilde, *Integral equation methods for scattering by infinite rough surfaces*, Math. Methods Appl. Sci., 26 (2003), pp. 463–488.
[54] H. Zhang and B. Zhang, *A novel integral equation for scattering by locally rough surfaces and application to the inverse problem*, SIAM J. Appl. Math., 73 (2013), pp. 1811–1829.
[55] B. Zhang and H. Zhang, *Recovering scattering obstacles by multi-frequency phaseless far-field data*, J. Comput. Phys., 345 (2017), pp. 58–73.
[56] B. Zhang and H. Zhang, *Imaging of locally rough surfaces from intensity-only far-field or near-field data*, Inverse Problems, 33 (2017), 055001.
[57] B. Zhang and H. Zhang, *Fast imaging of scattering obstacles from phaseless far-field measurements at a fixed frequency*, Inverse Problems, 34 (2018), 104005.
[58] D. Zhang and Y. Guo, *Uniqueness results on phaseless inverse scattering with a reference ball*, Inverse Problems, 34 (2018), 085002.
[59] D. Zhang, Y. Guo, J. Li, and H. Liu, *Retrieval of acoustic sources from multi-frequency phaseless data*, Inverse Problems, 34 (2018), 094001.